LA-3439-MS

LOS ALAMOS SCIENTIFIC LABORATORY
of the
University of California
LOS ALAMOS • NEW MEXICO

Graphs of Calculations of Energy Deposition and Air Fluorescence from Radiation Produced by a Nuclear Explosion in Space

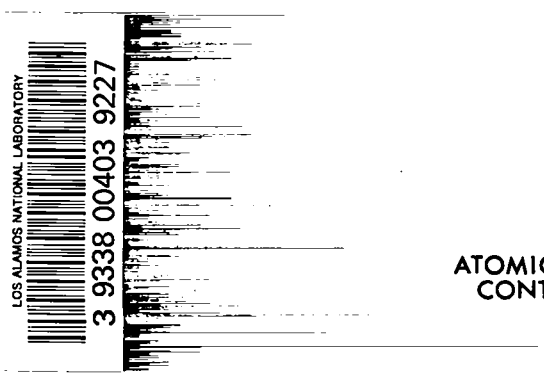

UNITED STATES
ATOMIC ENERGY COMMISSION
CONTRACT W-7405-ENG. 36

Printed in USA. Price $3.00. Available from the Clearinghouse for Federal Scientific and Technical Information, National Bureau of Standards, United States Department of Commerce, Springfield, Virginia

LA-3439-MS
UC-34, PHYSICS
TID-4500

LOS ALAMOS SCIENTIFIC LABORATORY
of the
University of California
LOS ALAMOS • NEW MEXICO

Report written: November 1965
Report distributed: April 22, 1966

Graphs of Calculations of Energy Deposition and Air Fluorescence from Radiation Produced by a Nuclear Explosion in Space*

by

E. W. Bennett

*Part of this work done under ARPA Order 631, Program Code No. 5820.

ABSTRACT

Results of calculations of energy deposition in the atmosphere and air fluorescence produced by x rays from a hypothetical nuclear explosion at an altitude of 10^5 km are presented in graphical form. The calculations were done for many parameters with the intent that the results would be useful in the detection of nuclear explosions in space, for example in systems design and signal interpretation, and in the prediction of atmospheric effects brought about by a high-altitude nuclear explosion.

The machine codes used in performing the calculations are described briefly. In all cases an x-ray yield of 1 kt was assumed.

Deposition calculations were done for a variety of source temperatures and incident photon energies ranging from a low temperature of 0.1 keV to a high temperature of 10 keV and for photon energies of 100 keV and 1 MeV. Deposition per unit volume as a function of altitude directly above a ground-based observer is presented for two cases: (1) burst at zenith, and (2) burst on the horizon. In the zenith case, the peak deposition varies only slightly with source temperature or photon energy, ranging between 2×10^{-15} and 0.8×10^{-15} joules cm^{-3}. The altitude of peak deposition, however, changes from 108 km for the 0.1 keV source to 80 km for the 1 keV source and 24 km for the 1 MeV photon source. For burst on the horizon, the peak deposition is lower by about two orders of magnitude, varying slightly about a value of 10^{-17} joules cm^{-3}, while the altitude of peak changes from 145 to 100 to 50 km for the 0.1 keV, 1 keV, and 1 MeV sources, respectively.

Air fluorescence calculations were done for a variety of source temperatures, detector fields of view, and burst directions as seen by an observer on the ground. An x-ray energy deposition conversion to fluorescence radiation efficiency of 1.4% was used.

The peak flux density recorded by an all-sky lens pointed at the zenith for burst at zenith varies from 10^{-7} W cm^{-2} for a 5 keV source to 0.6×10^{-7} W cm^{-2} for a 0.1 keV source. The flux is down by a factor of two in $\sim$ 250 μsec. For burst 80° from zenith (10° above the horizon) the peak flux density ranges from 10^{-8} W cm^{-2} to 4×10^{-8} W cm^{-2} and does not vary greatly during the calculated time span of 250 μsec.

Graphs of the incident flux density as a function of time from 10 μsec to 250 μsec are given for burst locations ranging from zenith to 80° from zenith for detectors with fields of view 90°, 120°, and 160° in diameter, for a source temperature of 1 keV. Depending on burst location and field of view, the peak varies from a high of 8×10^{-8} W cm^{-2} to a low of 2.5×10^{-9} W cm^{-2}.

Space-resolved and time-resolved plots of the air fluorescence apparent surface brightness as seen from the ground are presented for several burst locations. Peak brightnesses vary from 1.5×10^{-6} W cm^{-2} ster^{-1} to 5×10^{-9} W cm^{-2} ster^{-1} with typical values lying between 5×10^{-7} and 5×10^{-8} W cm^{-2} ster^{-1}.

ACKNOWLEDGMENTS

The EDS and HAF codes used for these calculations were developed to provide predictions and analysis assistance for field data acquired by LASL on high-altitude nuclear events during Operation Hardtack (1958) and Operation Dominic (1962). Most of the results given here were collected under the direction of H. Hoerlin for presentation at the Vela Summer Study conferences sponsored by ARPA in the summer of 1964. The nominal (1 kt) calculations were done at different times during the last several years; however, most of them were done in 1964 and a few in 1965. The machine codes were written by R. W. Humphrey and R. L. Yoakum, both of Group J-10, LASL.

CONTENTS

GRAPHS (continued) Page

Plots of air fluorescence expanding ring geometry: apparent surface brightness as a function of line of sight at several times after burst for five burst locations. Burst altitude: 10^5 km; x-ray yield: 1 kt; source temperature: 1 keV; fluorescence efficiency: 1.4%. Profiles plotted for times of 10, 20, 40, 80, 120, 160, 200, and 240 μsec.

INTRODUCTION

A variety of codes for machine calculations have been written to assist in the interpretation of data on prompt air fluorescence excited by radiation from high-altitude nuclear explosions. These codes have been used to predict energy deposition in the atmosphere and air fluorescence brightness due to radiation from a hypothetical nuclear explosion occurring at an altitude of 10^5 km. Graphs giving some of the results of these calculations for x rays are presented in this report.

The calculations were done to provide signal input information for use in the design of a ground-based detection system for nuclear explosions in space ("Vela Sierra").

X-ray energy deposition in the atmosphere as a function of altitude is taken from EDS calculations. Light received on the ground from air fluorescence excited by x rays is calculated by the HAF code. These codes, both written for the IBM 7094, are briefly described below.

THE EDS CODE

The EDS code computes energy deposition per unit mass and energy deposition per unit volume, respectively, according to the equations

$$E_M = \frac{Q(M)}{r^2} \quad , \quad \text{joules g}^{-1},$$

and

$$E_V = \frac{Q(M)\rho}{r^2} \quad , \quad \text{joules cm}^{-3},$$

where

r = the radius from the source, km,

ρ = air density at the point of deposition, g cm^{-3},

M = mass of air per unit area traversed between the source and the deposition point, g cm^{-2}, and

Q = source function, joules km^2 g^{-1}.

The function Q includes the (isotropic) source strength, the x-ray spectrum, and the attenuation due to absorption in the atmosphere. Q(M) is input in the form of a table of numbers and is calculated by other machine codes; this will be discussed further.

The geometry used in EDS is illustrated in Fig. 1. Burst altitude is specified and energy deposition calculated along a radius r at an angle θ with respect to the vertical through burst point. A spherical

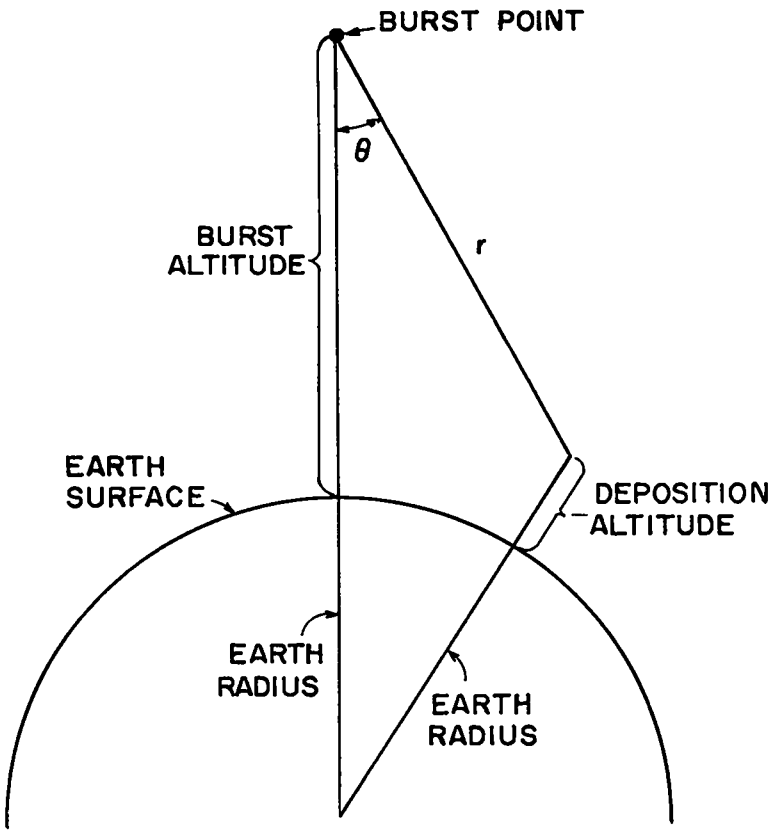

Fig. 1. EDS geometry.

earth is assumed. Air density as a function of altitude is input as a table of numbers. The quantity M is calculated by

$$M = \int_0^r \rho d\ell, \quad \text{g cm}^{-2},$$

where ℓ is measured along R.

The source function Q for x rays is calculated by a machine code called XRA. Q is determined for selected values of M by integrating over the Planckian appropriate for the source temperature(s) assumed. Mass absorption coefficients for air as a function of x-ray wavelength are input as a table of numbers. XRA will compute Q(M) tables given a source radiating a specified amount of energy at a constant temperature; provision is made for the temperature and radius of the source to vary as a function of time as in an actual case calculated by still other codes in use at Los Alamos.

In all of these calculations contributions due to scattering are neglected. Scattering becomes important for photon energies $\geq \sim 12$ keV.

THE HAF CODE

Only a brief description of the HAF calculation is given here. A detailed write-up, including assumptions and derivation of equations, is contained in Report LA-3409-MS Supplement.[1]

Energy deposition in the atmosphere is assumed to produce energetic primary electrons which in turn produce less energetic secondary electrons. Fluorescent emission is assumed to occur instantaneously upon excitation by the primary and secondary electrons. The total energy, B_V, per unit volume radiated as air fluorescence is taken to be isotropic and proportional to the energy, E_V, deposited per unit volume according to the equation

$$B_V = \eta E_V \quad , \quad \text{joules cm}^{-3},$$

where the constant of proportionality, η, is called the "fluorescence

efficiency." The rate at which energy B_V is emitted at a point in space is assumed proportional to the number of primary electrons present with sufficient energy to excite fluorescence, with emission occurring uniformly during the primary electron slowing-down time. The x-ray source pulse is assumed to be square, lasting a finite time. Thus the time history of emission of energy B_V at a point in space is found by folding together the source pulse time duration and the electron slowing-down time. Energy deposition is assumed to be "local."

There is another time effect for a ground-based detector called "geometrical time smear." This effect is due to the fact that the path length for radiation traveling at the velocity of light from burst point to the point of energy deposition and thence to a detector on the ground depends on the line of sight of the detector and on the altitude at which deposition occurs. Geometrical time smear is by far the dominant effect in the calculations reported here for all lines of sight passing more than a few degrees from the line of sight to burst.

The fluorescence efficiency, η, is assumed to vary with air density, ρ, and hence with altitude, H, according to the expression

$$\eta = \frac{\eta_o}{1 + \rho/\rho_o} \quad ,$$

where η_o is a constant (discussed below) and $\rho_o = 1.82 \times 10^{-5}$ g cm^{-3}. This value of ρ_o is based on measurements reported by Grün.[2] With increasing altitude, η approaches η_o and is essentially equal to η_o at altitudes $\geq \sim 40$ km (for this value of ρ_o). While there is some question about the accuracy of this value for ρ_o, the question is probably academic, since, for the conditions considered here, most of the fluorescent emission comes from altitudes > 60 km where $\eta \doteq \eta_o$. The value of ρ_o would have to be high by more than a factor of 10 to affect the accuracy of the calculations appreciably.

The electron slowing-down time is a function of the air density and the hardness of the radiation. Average slowing-down times for a suitable

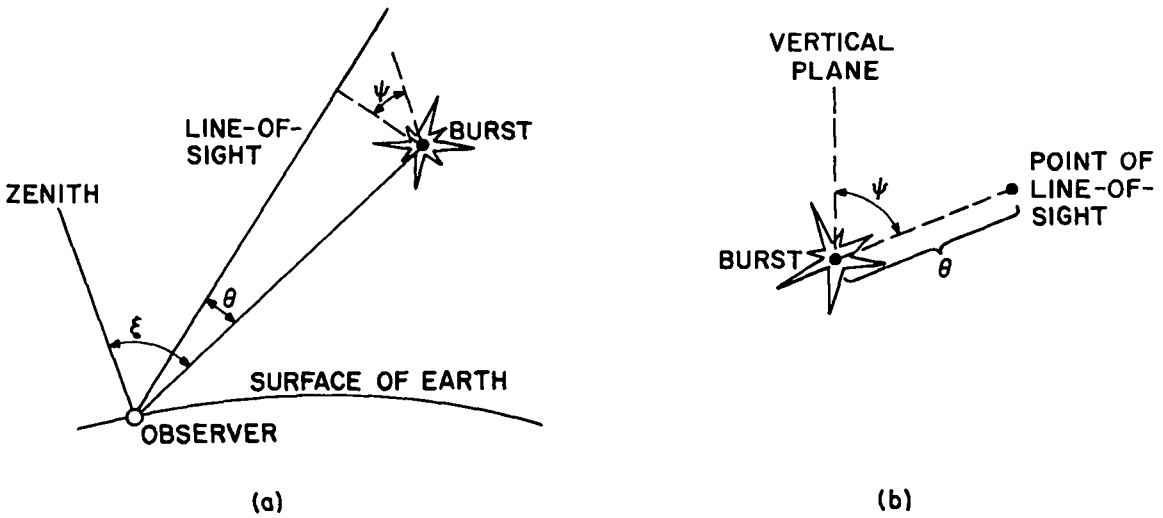

Fig. 2. Diagram showing HAF coordinates. (a) Side view showing polar axis L and angles ξ and θ. (b) View looking toward burst point from the observing station showing the angles ψ and θ.

density have been calculated by hand using the x-ray spectra computed for various values of M. Results are input to HAF as a table of numbers from which a slowing-down time is calculated by scaling inversely with the density. Because of the filtering effect of the air, the x-ray spectrum increases in hardness with increasing M.

Figure 2 is a diagram showing the coordinate system used in HAF. A spherical polar coordinate system is set up with the polar axis the line from ground-based observer to burst point. This axis is tilted an angle ξ from the vertical at the observer. The line of sight is at an angle θ from the polar axis and rotated an angle ψ about the polar axis. ψ is measured from the vertical plane through burst point and the observing station. A line of sight passing directly above burst point would have $\psi = 0$, one passing directly below burst would have $\psi = 180°$,

and one passing on a horizontal line to one side of burst would have $\psi = 90°$. See Fig. 2(b). Light is received at the observer at a time t from a distance R along the line of sight from radiation deposited at a distance r from burst.

In the calculation, values of θ and ψ are selected and the brightness, B (W cm^{-2} $ster^{-1}$), is calculated for various values of t. The time t = 0 is the time of arrival at the observer of the leading edge of a pulse traveling at the velocity of light along the shortest path from burst to the observer (L).

If a number of different values of θ and ψ are specified, so that a "mesh" is defined across a portion (or all) of the sky, the code will integrate B over the coordinates θ and ψ to obtain energy flux density, W cm^{-2}, incident at the observer as a function of time.

As indicated in Fig. 2, the earth is assumed to be spherical.

Q(M) and ρ(H) information needed in the HAF calculation is input as tables in the same format as used in EDS.

VALUES OF PARAMETERS

Mass absorption coefficients of air used in computing the Q tables were taken from a Rand report by Gilmore.[3] Air-density values as a function of altitude were the "average" numbers listed in CIRA 1961.[4]

The value of η_0 used in the HAF calculations reported here was the pre-Dominic value, $\eta_0 = 0.014$. For ease of comparing results it was decided to continue to use this number until a new value was extracted from the Dominic data. A "best" value is now available[5] and is quoted as $\eta_0 = 0.045\ ^{+0.045}_{-0.023}$, where the uncertainty is thought to be within a factor of two.

Air fluorescence radiation from high-altitude nuclear explosions consists principally of band emission from three systems of molecular nitrogen: (1) the N_2 second positive system (mostly near ultraviolet), (2) the N_2^+ first negative system (mostly visible in the blue), and (3) the N_2 first positive system (mostly near infrared). There is evidence

that the energy radiated is partitioned approximately equally among these three systems.

A band of considerable interest in the detection problem is the $(v',v'') = (0,0)$ transition in the N_2^+ first negative system with bandhead at 3914 Å. The high-altitude efficiency for this band is quoted[5] as $\eta o_{3914} = 0.01$, where the uncertainty factor is the same as that given above.

Thus, in using the graphs plotted here to obtain predicted air fluorescence signals, a "total" light prediction is found by multiplying the ordinate by ~ 3; a prediction for one of the molecular systems, by taking the results "as is"; and a prediction for the 3914 Å band, by multiplying the ordinate by 2/3.

All calculations included here were done for an assumed x-ray yield of 1 kt = 10^{12} cal $\doteq 4.2 \times 10^{19}$ ergs at an altitude of 10^5 km radiating at a constant temperature.

EDS GRAPHS

Energy deposition as a function of altitude directly above a ground-based observer is given for two cases: burst at zenith and burst on the horizon. Because of general interest in the altitude of peak deposition as a function of photon energy, calculations have been done for a variety of source temperatures (blackbody assumed) and a couple of monoenergetic gamma-ray photon energies.

Results should be accurate to within the accuracy of the mass absorption coefficients and the model atmosphere used for source temperatures of 0.1, 0.2, 0.4, and 1 keV, and, to a lesser extent, 3 keV. Neglect of scattering introduces considerable error into the 5 keV calculation, but values should be correct to within a factor of two.

The XRA code computes Q tables by determining the transmission through M g cm^{-2} of air as $e^{-\mu M}$, where μ, the mass absorption coefficient, is a function of the x-ray wavelength, and by taking the fraction of the energy deposited per gram to be given by μ. Thus, the contribution to Q

from x rays at a given wavelength is proportional to $\mu e^{-\mu M}$. When Compton scattering becomes important, at photon energies $h\nu \geq \sim 12$ keV, then the fraction of the energy deposited is given by the "true" mass absorption coefficient, μ_{TRU}, whereas the transmission, including absorption and scattering, is given by $e^{-\mu_{TOT} M}$ where the "total" mass absorption coefficient, $\mu_{TOT} > \mu_{TRU}$. Thus the contribution to Q from x rays of wavelength λ, neglecting scattering, is proportional to

$$\mu_{TRU}(\lambda) e^{-\mu_{TOT}(\lambda) M} .$$

Scattering can be included by means of a "buildup factor," $B(\lambda,M)$, so that the total contribution to Q is accurately proportional to

$$B(\lambda,M) \mu_{TRU}(\lambda) e^{-\mu_{TOT} M} ,$$

where $B \geq 1$, and is essentially the "right answer over the wrong answer." Buildup factors have been calculated[6] for gamma-ray energies between 0.25 and 10 MeV for a point isotropic source in an infinite homogeneous medium. These results were used in the 1 MeV EDS calculations given here without any other justification than that the method gave answers in agreement with Monte Carlo calculations for the special case of values of $M \leq 100$ g cm^{-2} and a source at a high altitude but low enough to be still in the atmosphere.[7,8]

No buildup factors are known to the author for photon energies in the range 12 to 250 keV. However, it can be plausibly argued that, just as the use of $\mu_{TOT} M$ as the exponent leads to a computed transmission that is too small, so the use of $\mu_{TRU} M$ should lead to a transmission that is too large (except for small M less than 1 mean free path), and that two calculations, using the two transmissions, should at least bound the correct answer above and below. Again, this argument is supported by results of Monte Carlo[9] calculations for the special cases of 40 keV and 50 keV source photons. Q(M) tables were calculated in this manner for the 100 keV photon source results given here.

In the 10 keV source temperature case, Q(M) tables were calculated with XRA. Provision is made for only one table of mass absorption coefficients in this code, so that the same number is used like a true mass absorption coefficient as the fraction deposited and like a total mass absorption coefficient to compute the transmission. However, this fact should not be of great importance, and, indeed, causes a change in the direction of decreasing the difference between the upper and lower bounds.

HAF PLOTS

A set of HAF calculations was done for a source temperature of 1 keV for burst locations at zenith and at angles of 20°, 40°, 60°, and 80° from zenith. In each case values of θ and ψ were chosen to define a mesh, and the results were integrated over θ and ψ to obtain flux density incident at the observer as a function of time for three hypothetical detectors. Time was varied from 10 to 250 μsec in 10 μsec steps.

The three detectors were assumed to be pointed at the zenith and differed only in fields of view, which were 90°, 120°, and 160° in diameter defining cones of half-angle 45°, 60°, and 80°, respectively. Detector response was assumed perfect out to the edge of the field of view, and zero beyond the edge.

The brightness, B, W cm^{-2} $ster^{-1}$, provides space resolution information, for example, for considerations involving image-forming optics or highly collimated systems. Plots of the brightness as a function of time are given for selected directions in space. For off-zenith burst locations, a line of sight described as an angle "up from burst" is for the angle $\psi = 0$. For example, for burst 40° from zenith, a line of sight 40° up from burst is pointing to zenith.

RING GEOMETRY

The "expanding ring" characteristic of air fluorescence has been found to be a useful tool in detection systems design. The geometry is illustrated in Fig. 3. Consider a very short pulse of radiation propagating outward from burst point. Deposition is assumed to occur in a thin layer and to produce fluorescence lasting for a time t_o at the point of deposition. As seen by a ground observer directly below burst, light arrives from the deposition layer only along the line of sight to burst at time $t = 0$. As time t increases to $t = t_o$, the region from which light is received appears to grow into a disc with the path t_o (see Fig. 3) corresponding to the edge of the disc where t_o is the difference in time required for light to travel the path t_o from the time required to travel the direct line to the observer. At time t_o the observer ceases to see light along the direct line of sight to burst, so that this region "goes out." Thus, at time $t_1 > t_o$, the observer receives light from a ring such that the travel time for light along t_1 is time t_1 longer than the travel time along the direct line. The travel time for

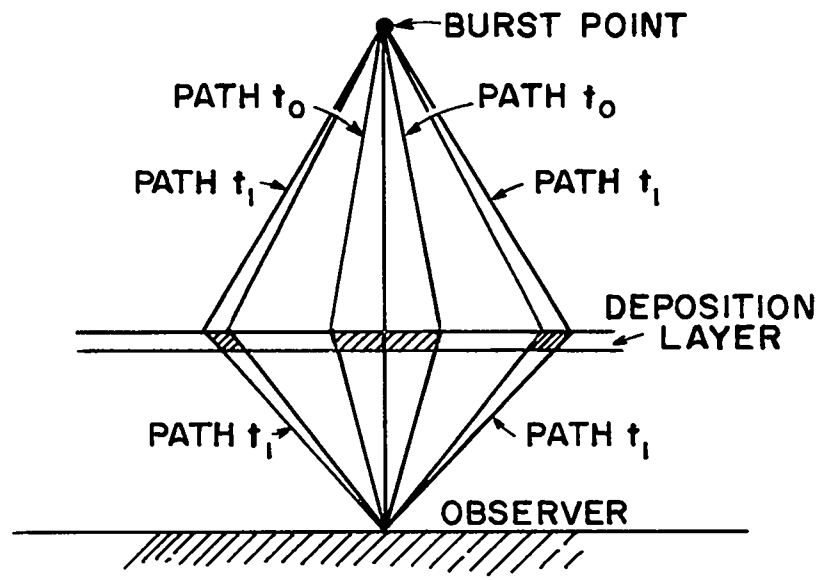

Fig. 3. Diagram of ring geometry.

the inner path of ring t_1 is t_o shorter than that for path t_1; for all paths shorter than this the fluorescence has "gone out." For a zenith burst the ring is circular.

Graphs illustrating the expanding ring have been constructed from the HAF calculations by plotting the brightness as a function of the angle θ at constant time. Because of the considerable depth of the deposition layer, the ring interior does not exactly "go out," and the edges of the ring are not sharply defined; the maximum brightness in the ring is, however, about an order of magnitude greater than the brightness in the interior.

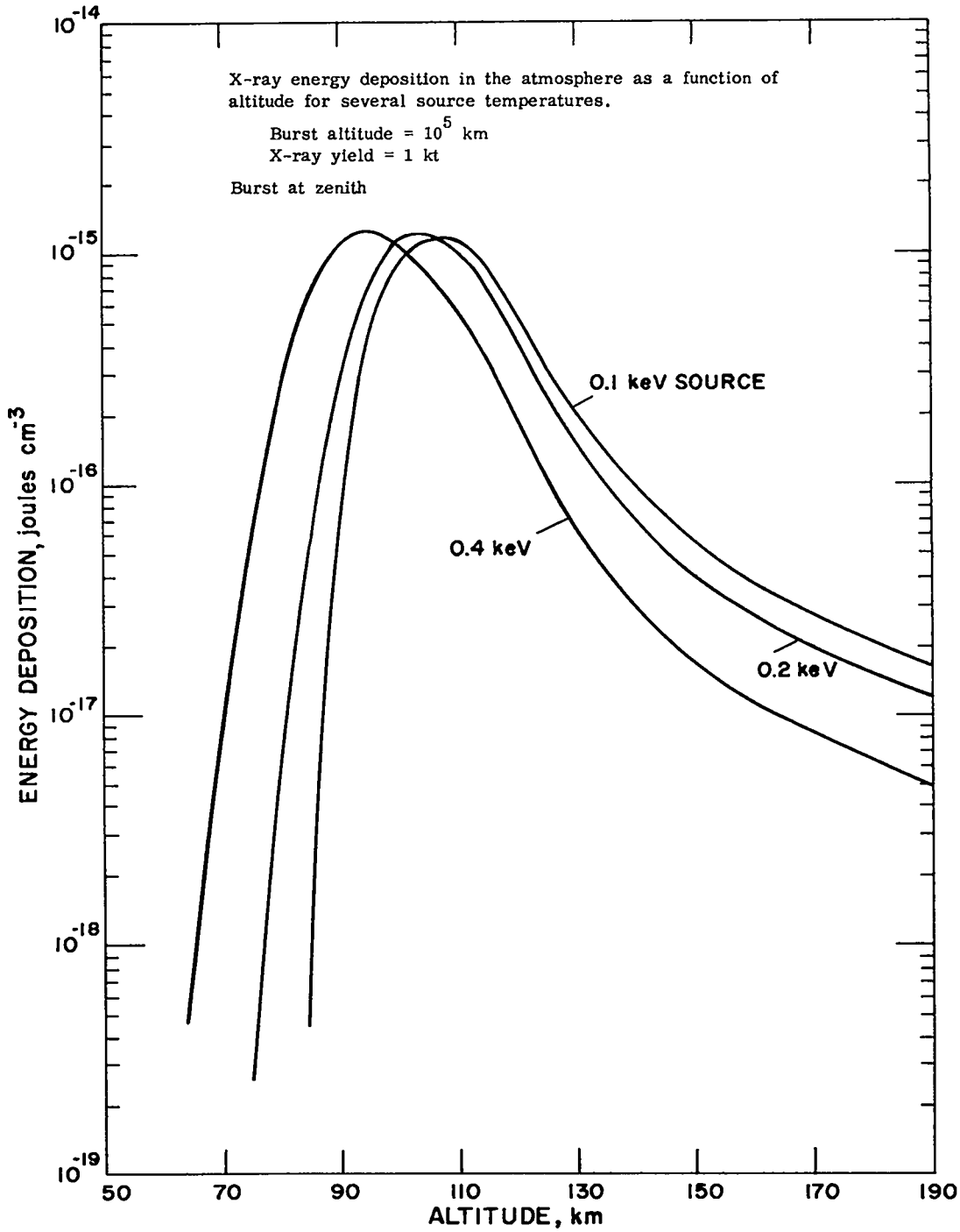

Graph 1 Source temperatures of 0.1, 0.2, and 0.4 keV

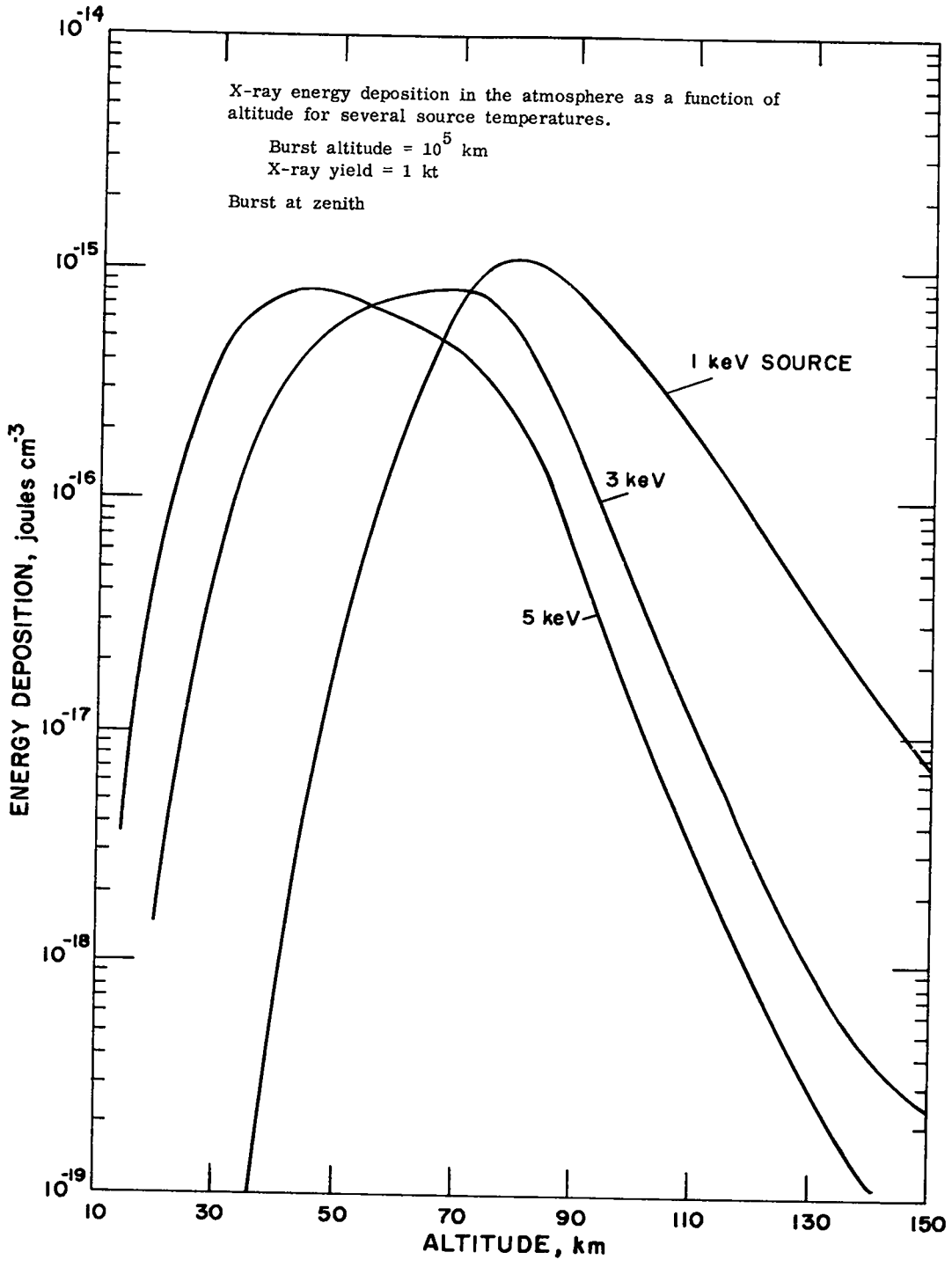

Graph 2 Source temperatures of 1, 3, and 5 keV

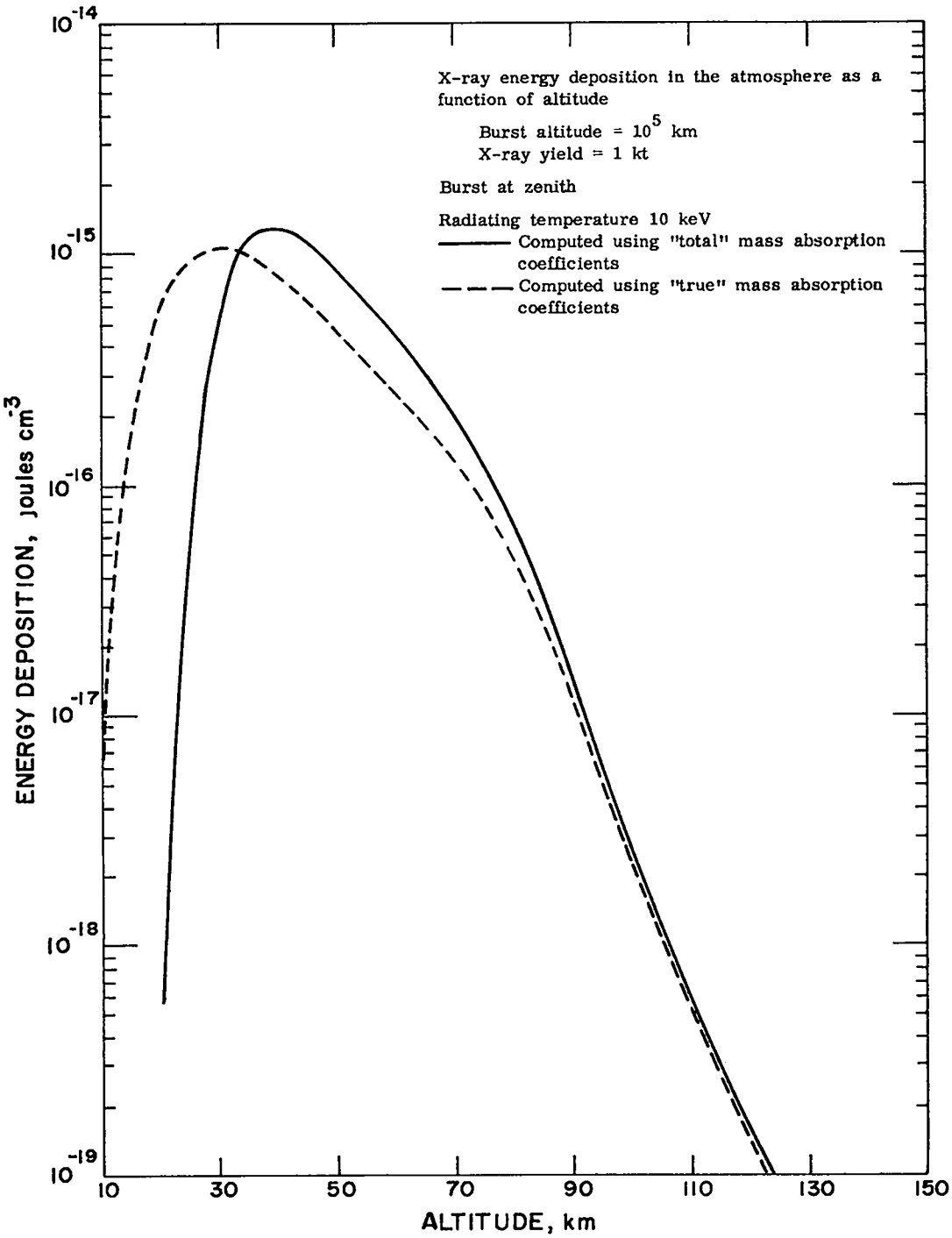

Graph 3 Source temperature of 10 keV (2 approximations)

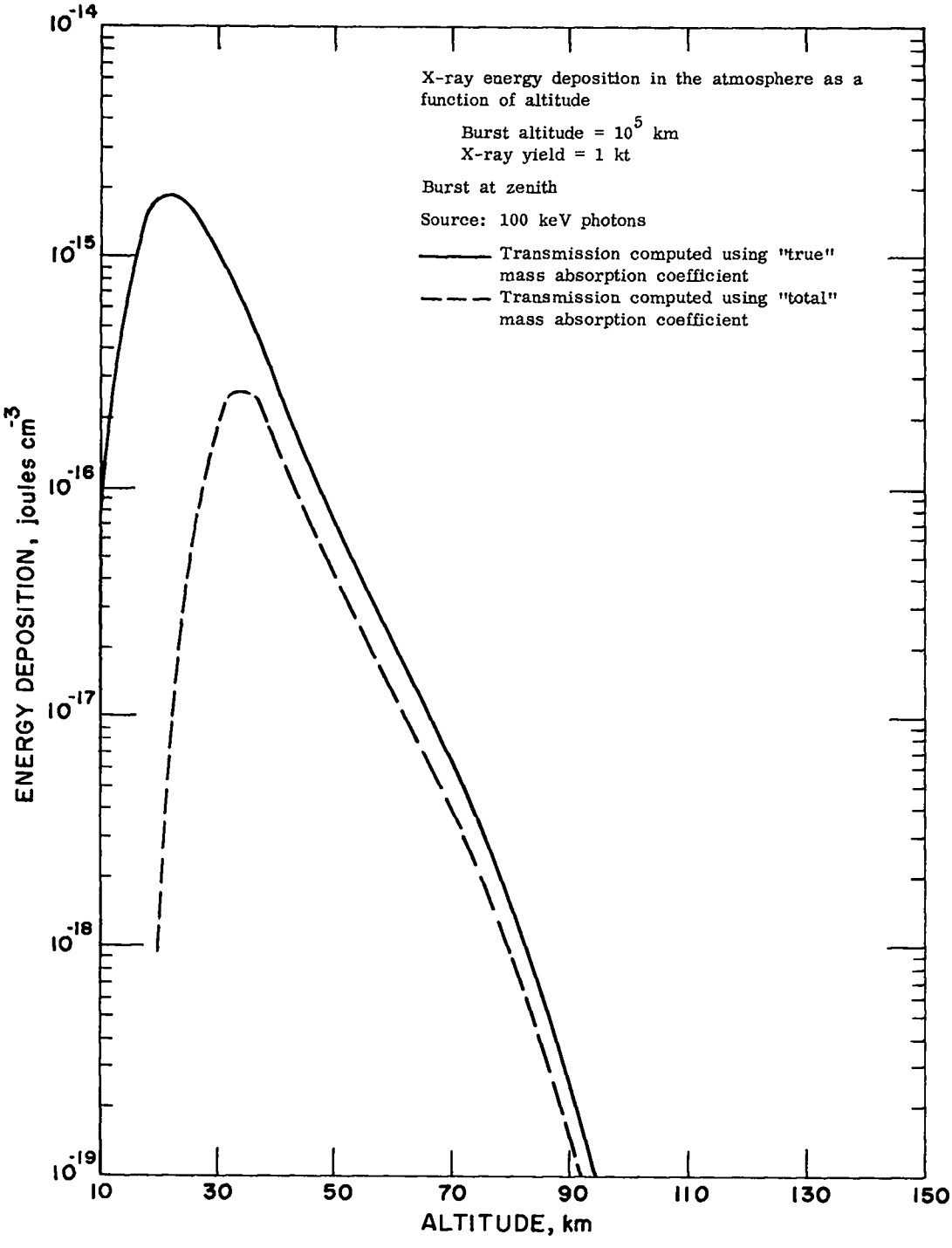

Graph 4 Photon energy of 100 keV (2 approximations)

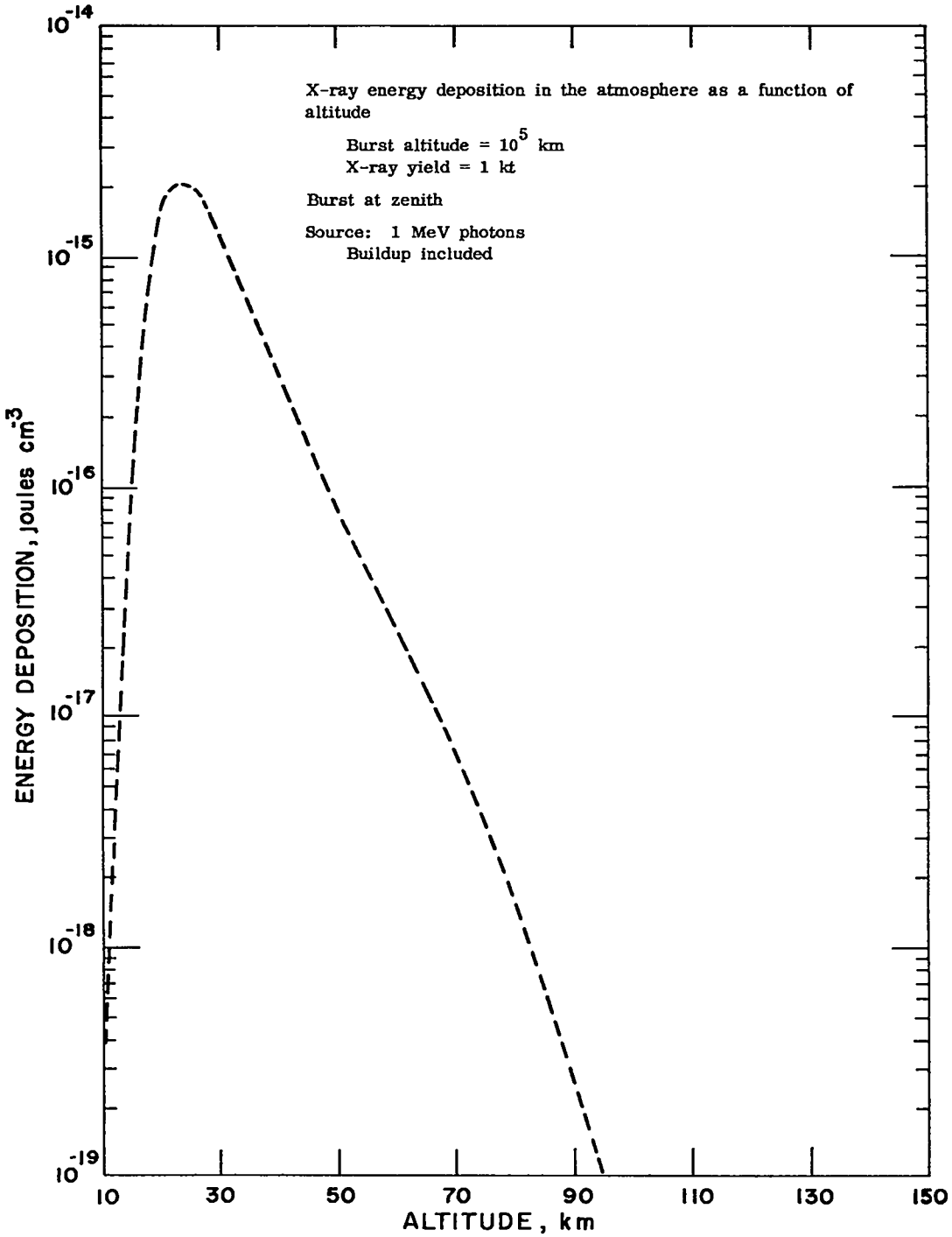

Graph 5 Photon energy of 1 MeV (buildup included)

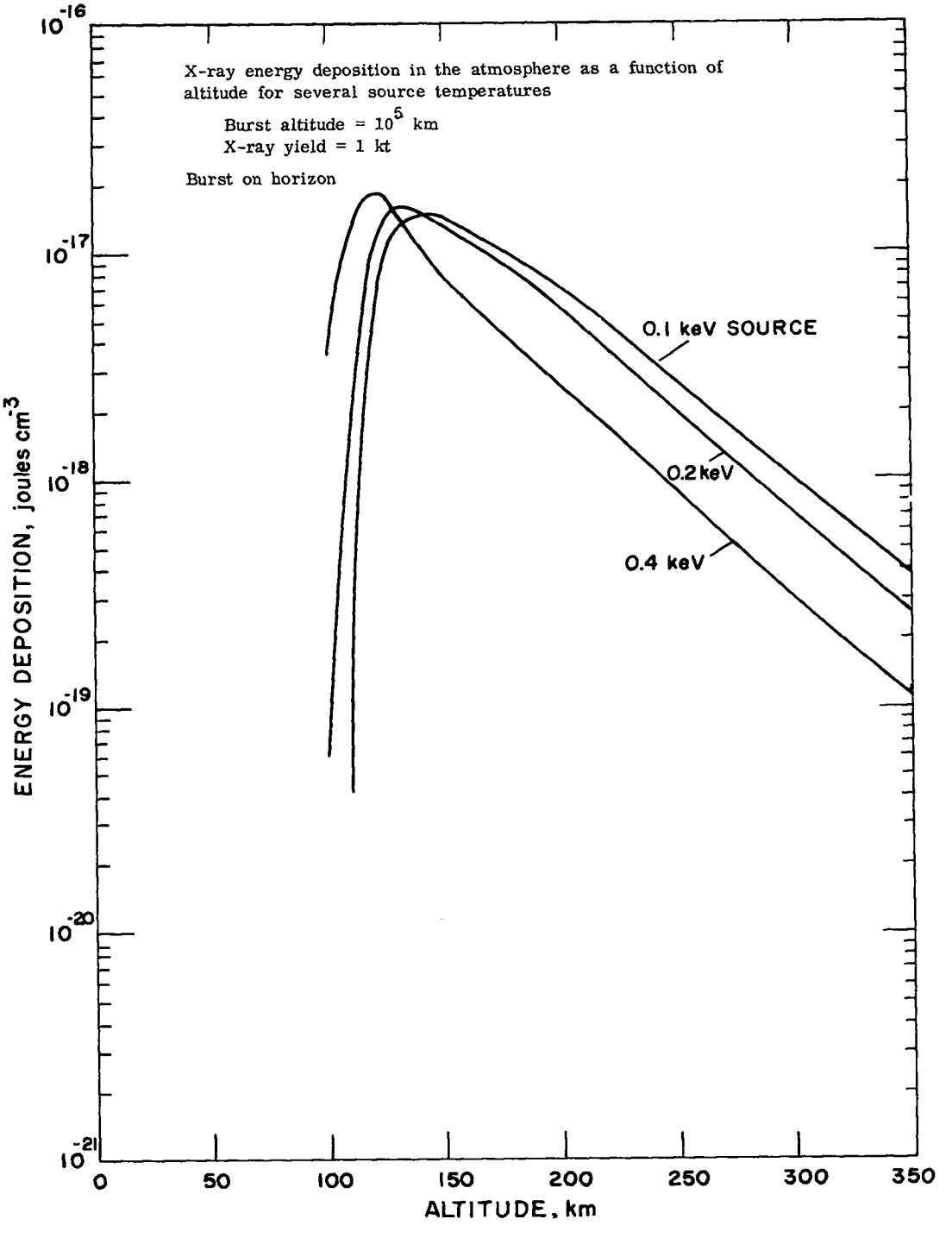

Graph 6 Source temperatures of 0.1, 0.2, and 0.4 keV

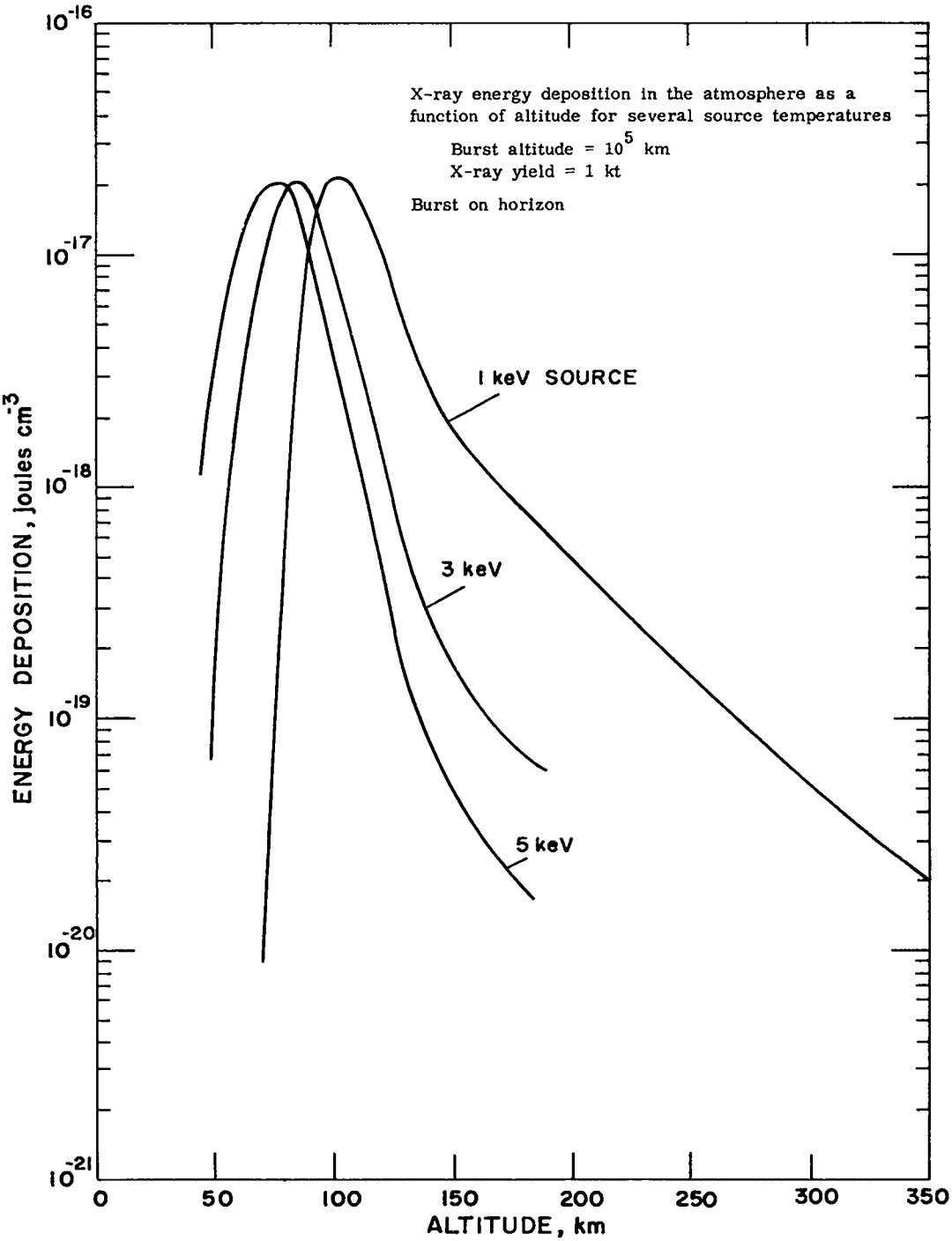

Graph 7 Source temperatures of 1, 3, and 5 keV

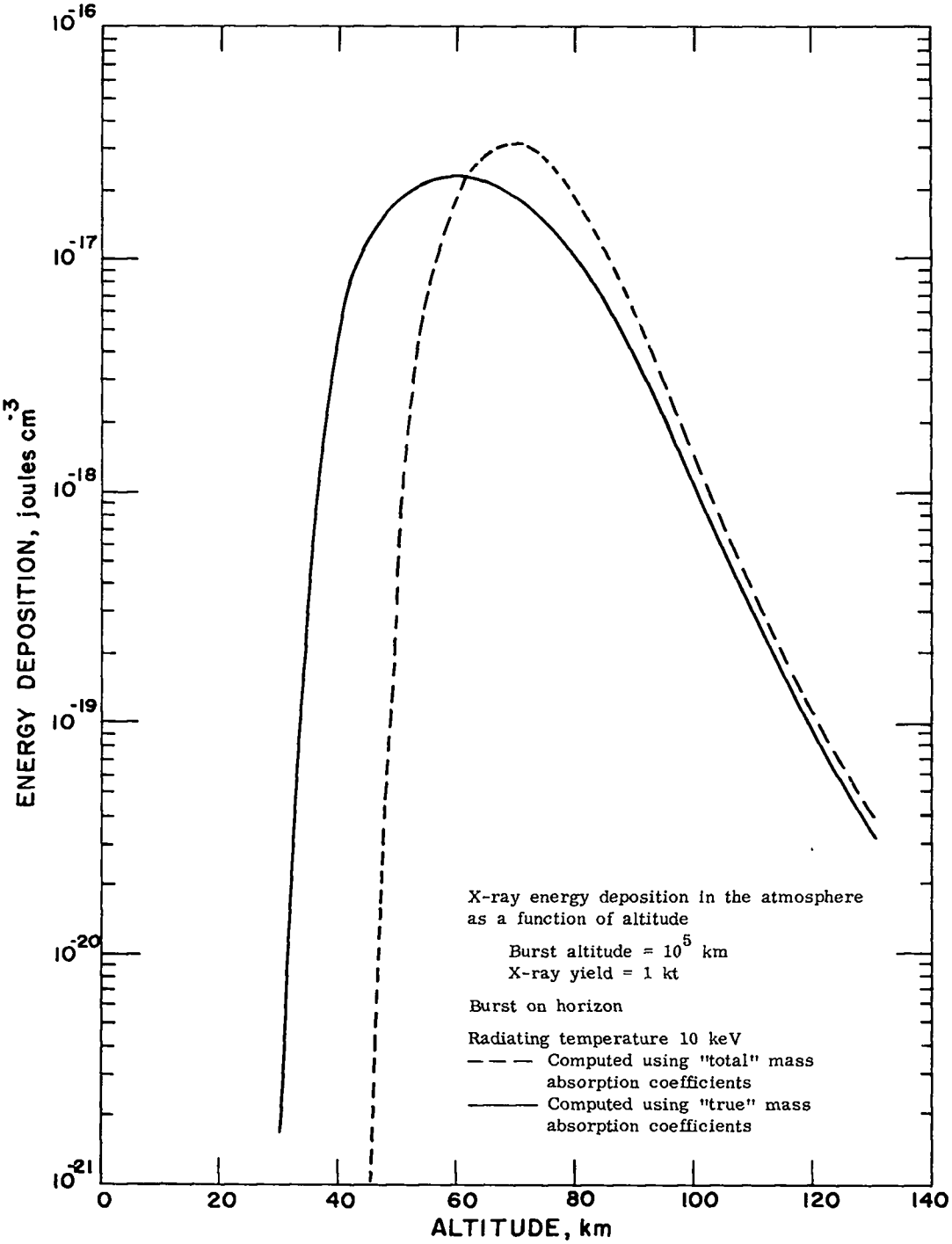

Graph 8 Source temperature of 10 keV (2 approximations)

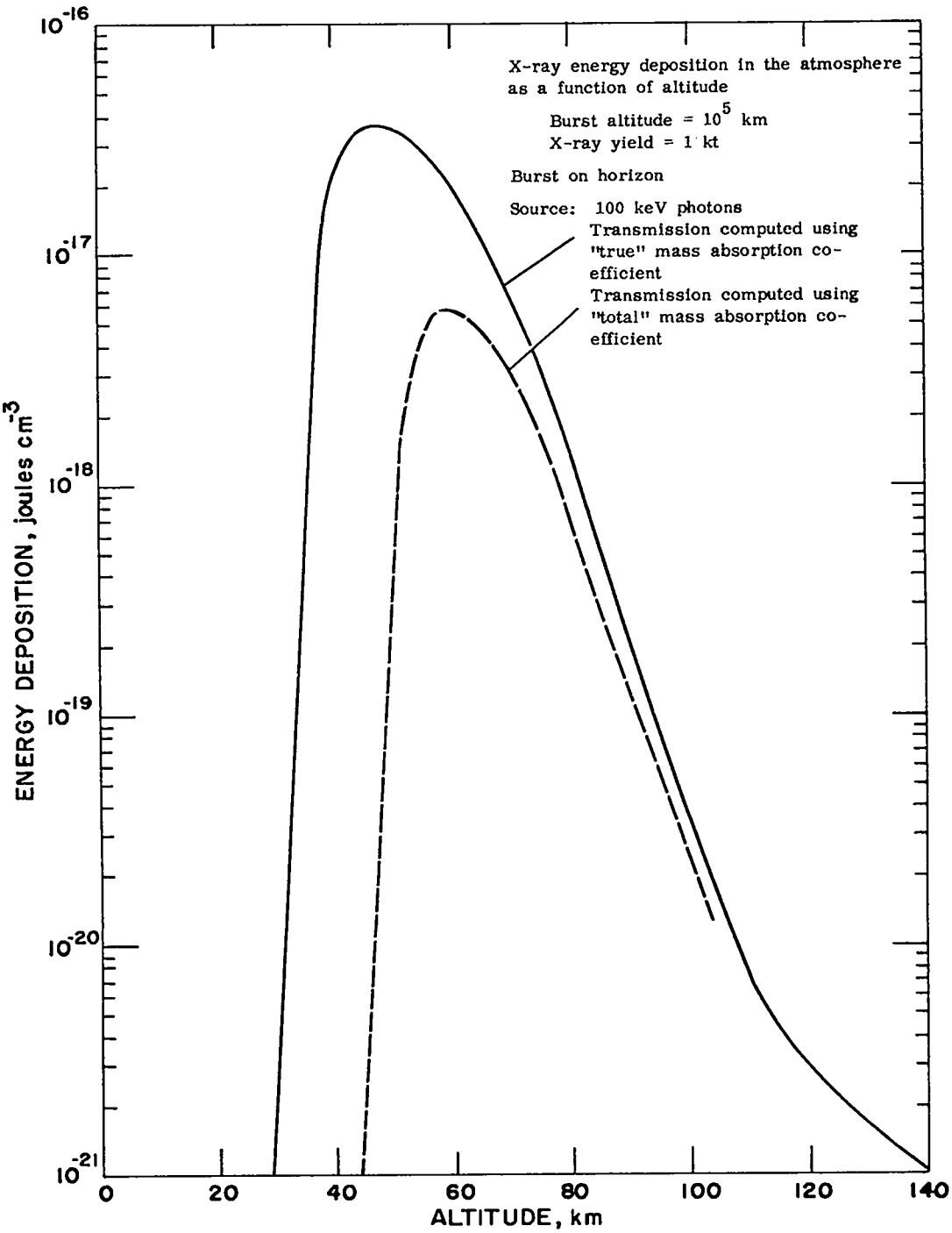

Graph 9 Photon energy of 100 keV (2 approximations)

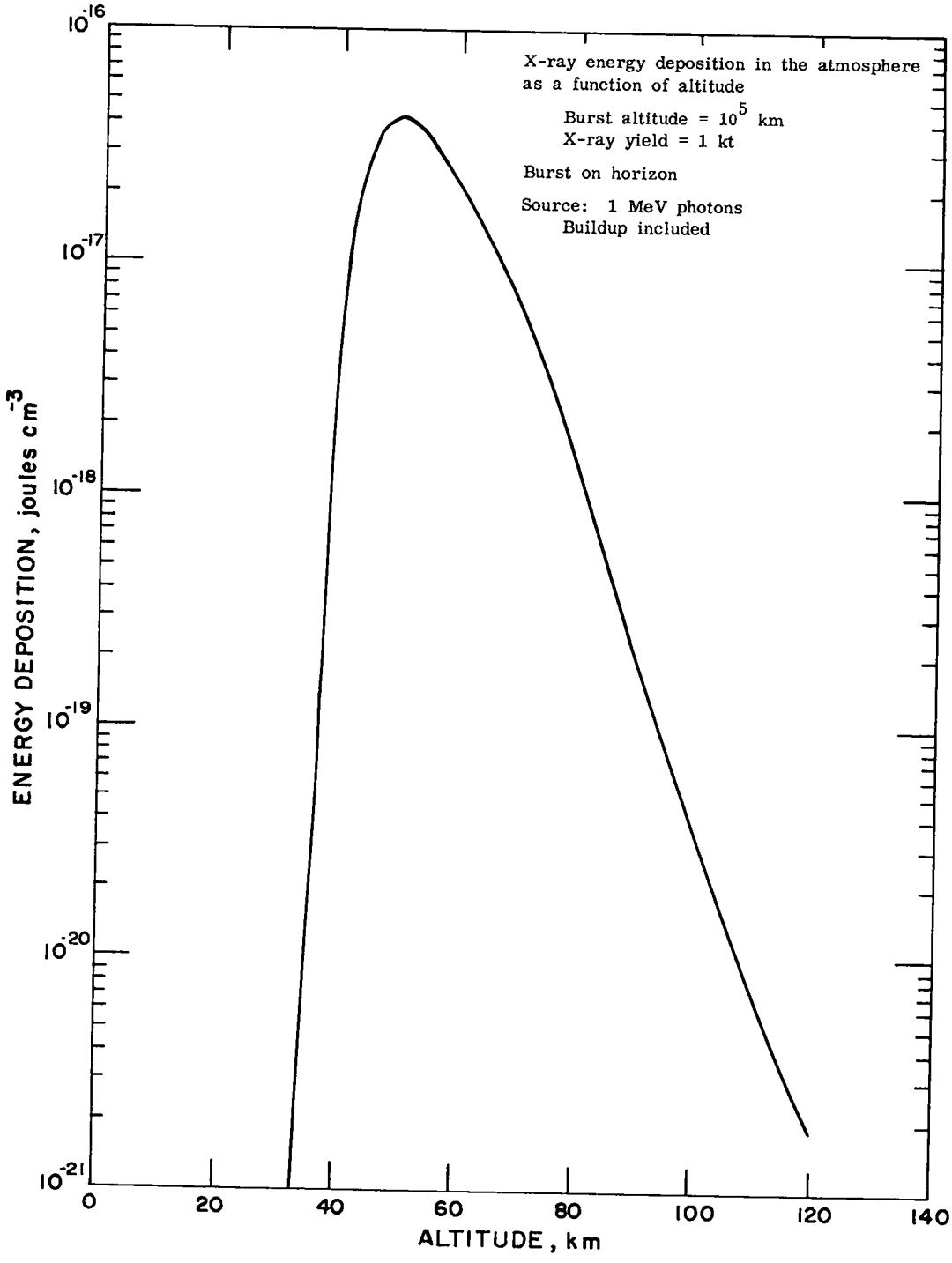

Graph 10 Photon energy of 1 MeV (buildup included)

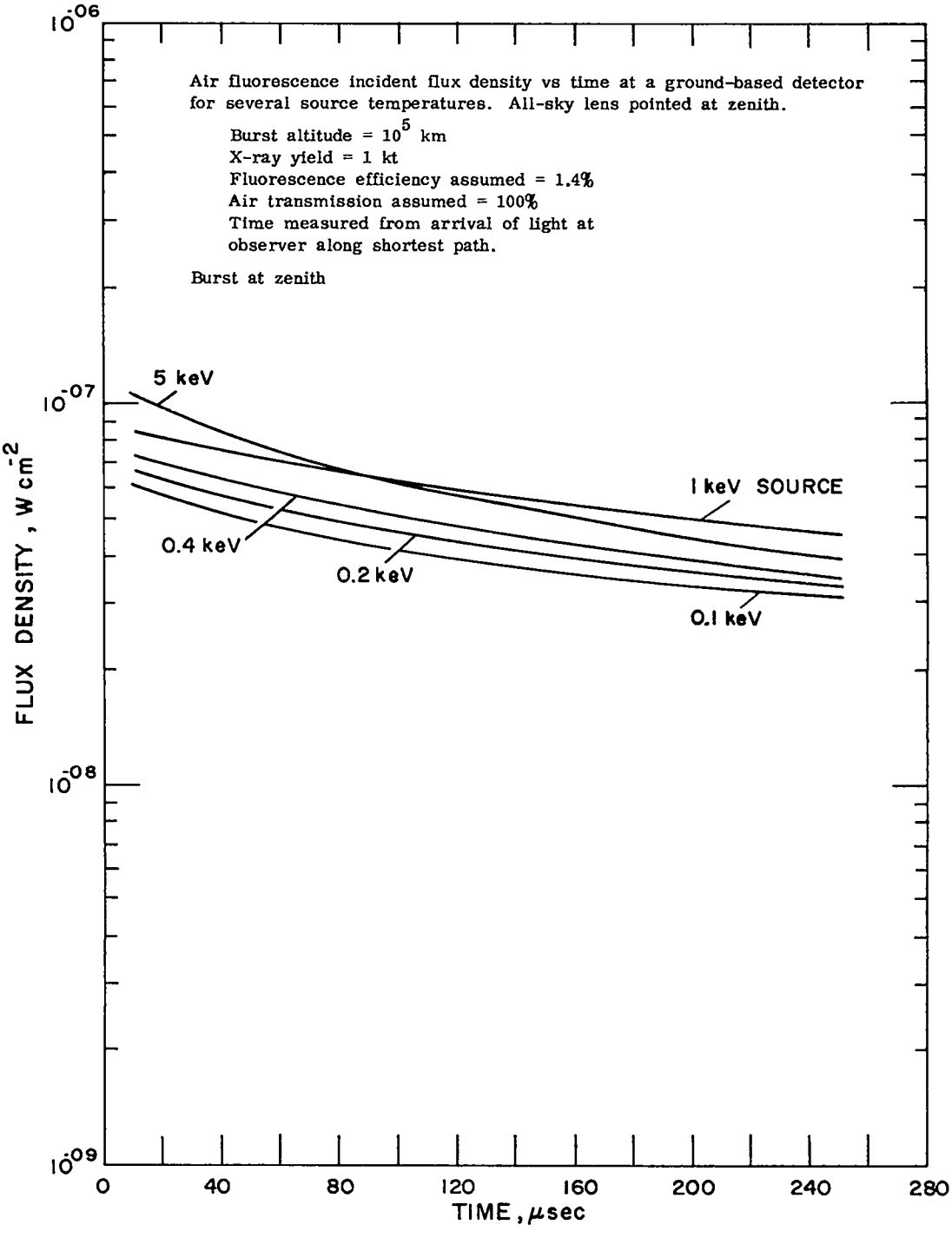

Graph 11 Source temperatures of 0.1, 0.2, 0.4, 1, and 5 keV

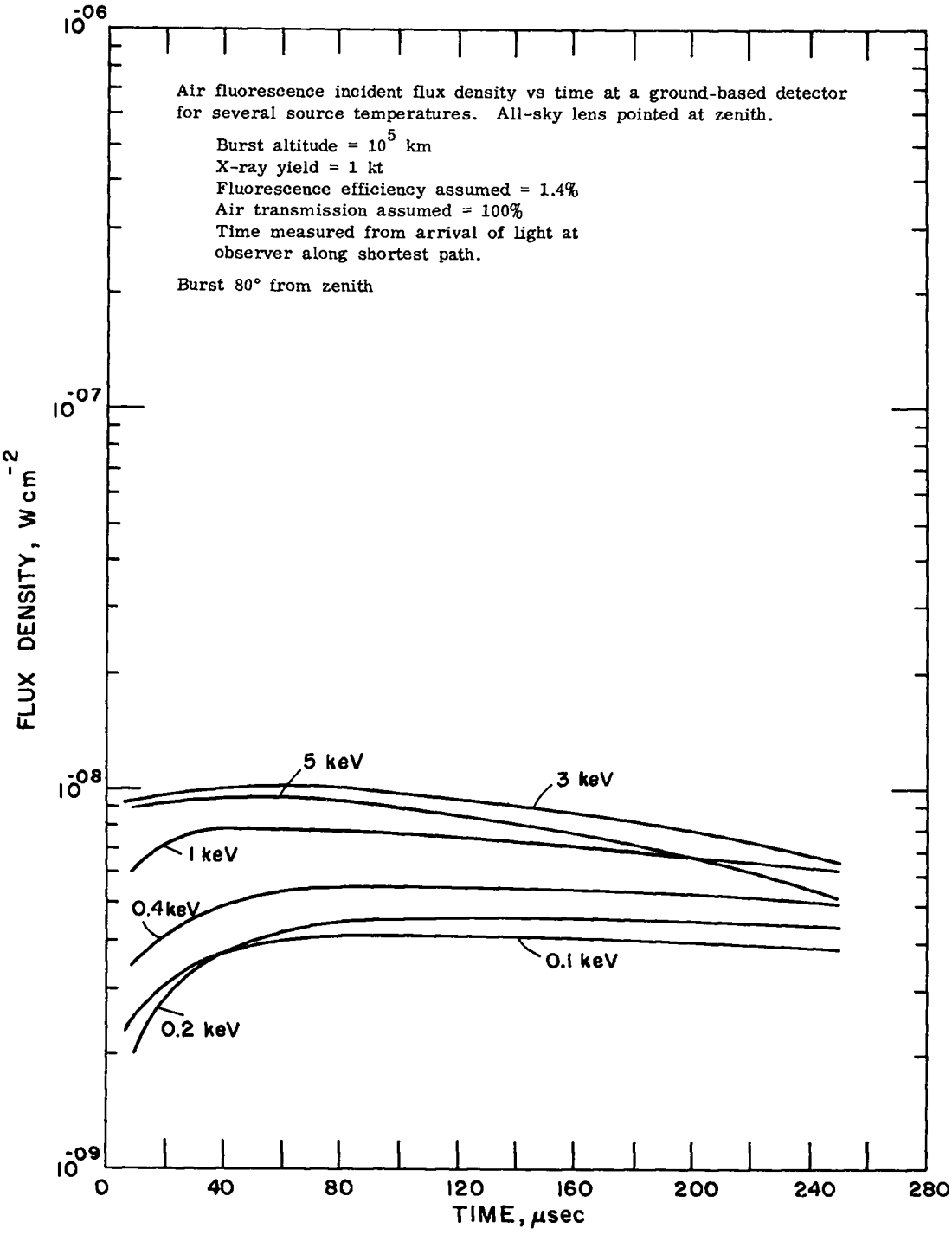

Graph 12 Source temperatures of 0.1, 0.2, 0.4, 1, 3, and 5 keV

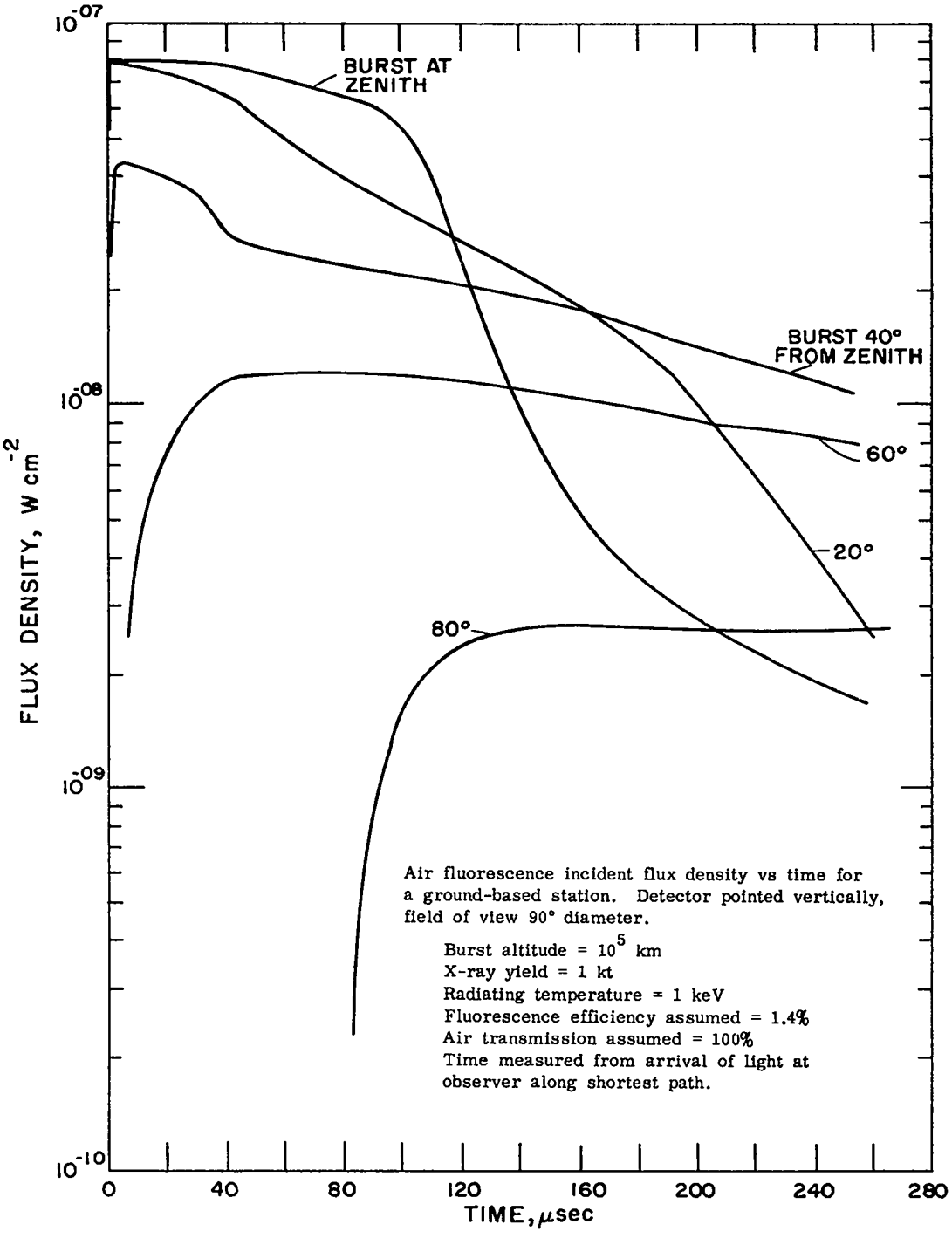

Graph 13 Field of view 90° diameter. Burst at zenith and at angles of 20°, 40°, 60°, and 80° from zenith

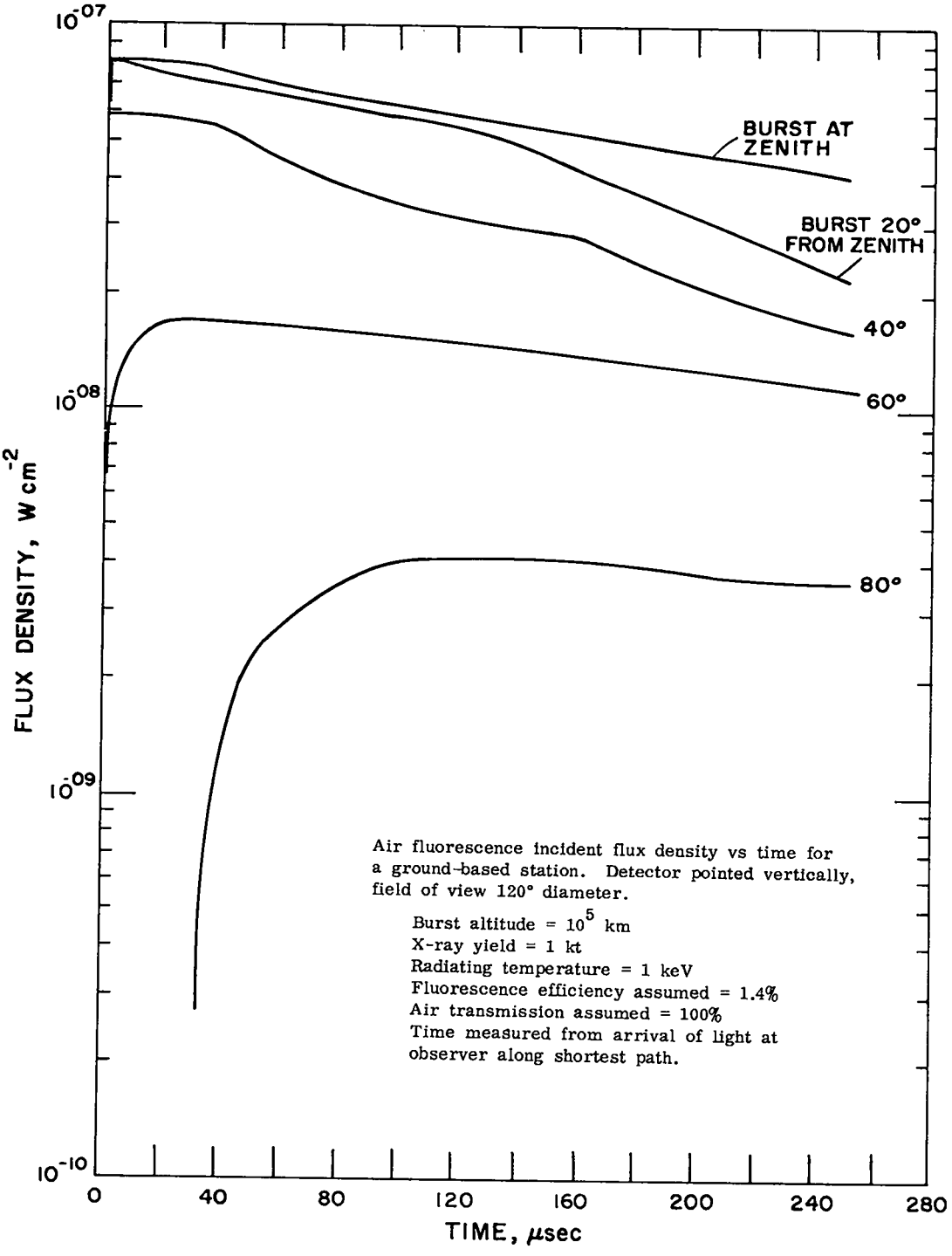

Graph 14 Field of view 120° diameter. Burst at zenith and at angles of 20°, 40°, 60°, and 80° from zenith

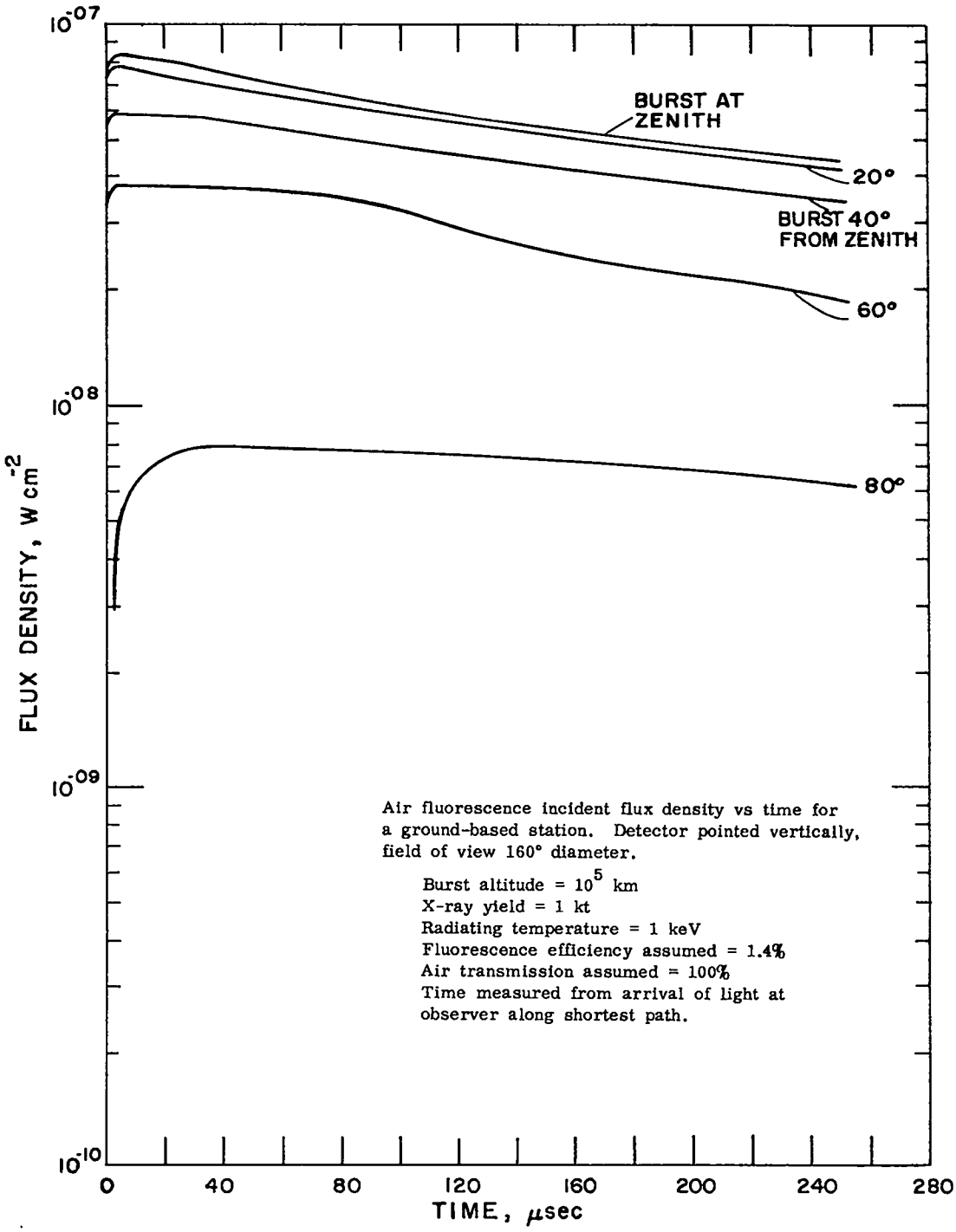

Graph 15 Field of view 160° diameter. Burst at zenith and at angles of 20°, 40°, 60°, and 80° from zenith

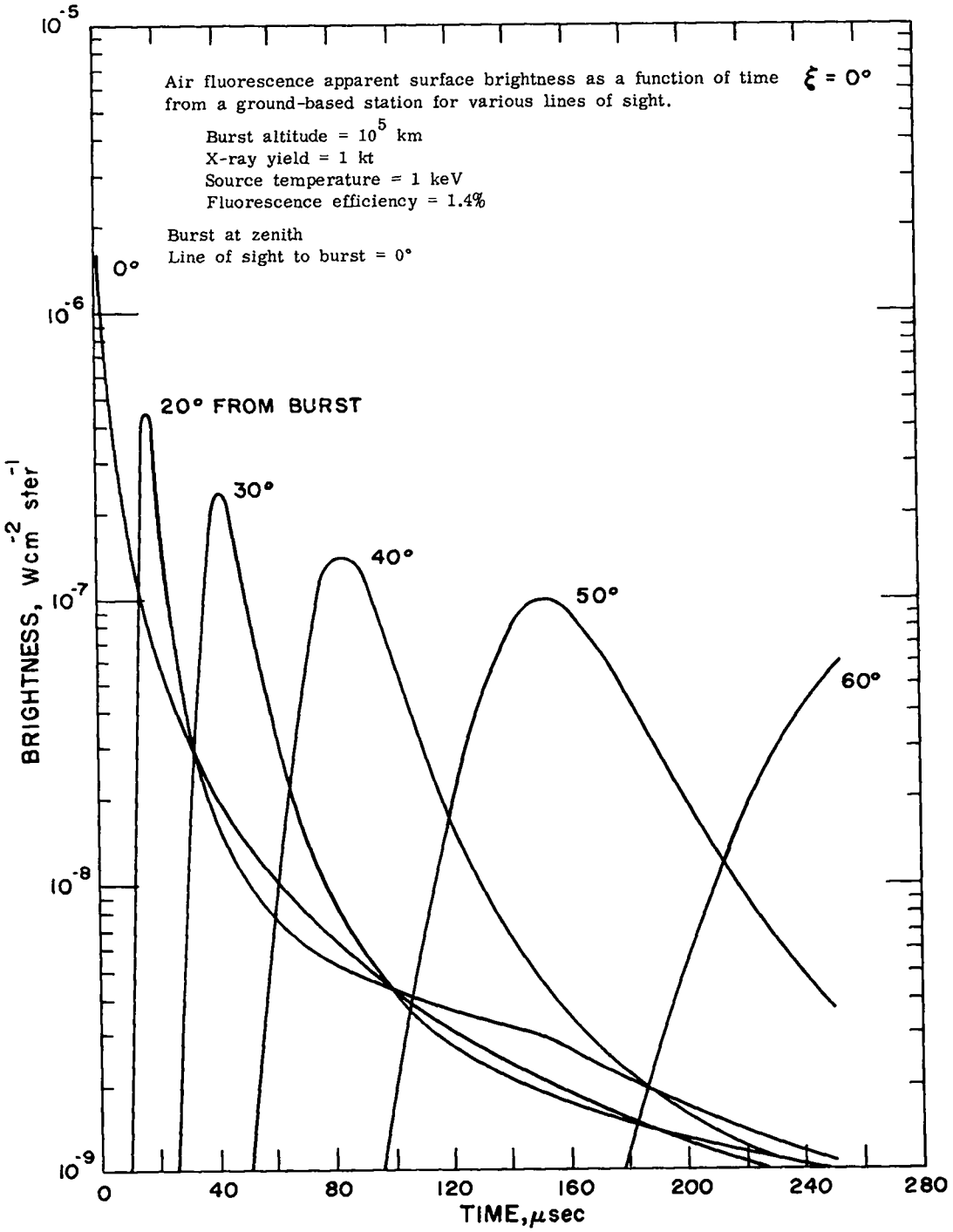

Graph 16 Lines of sight at angles of 0°, 20°, 30°, 40°, 50°, and 60° from burst

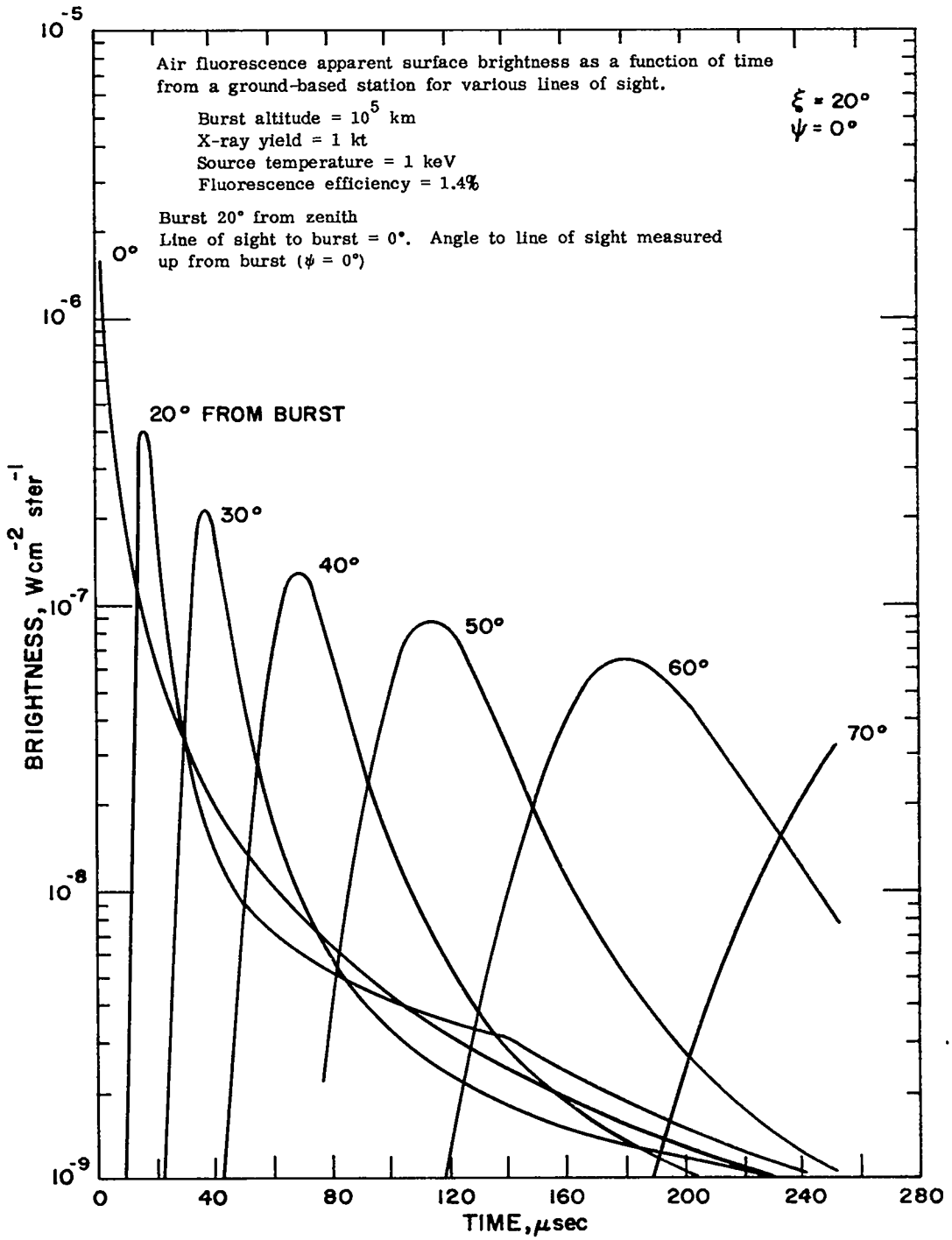

Graph 17 Lines of sight at angles of 0°, 20°, 30°, 40°, 50°, 60°, and 70° measured up from burst (ψ = 0°)

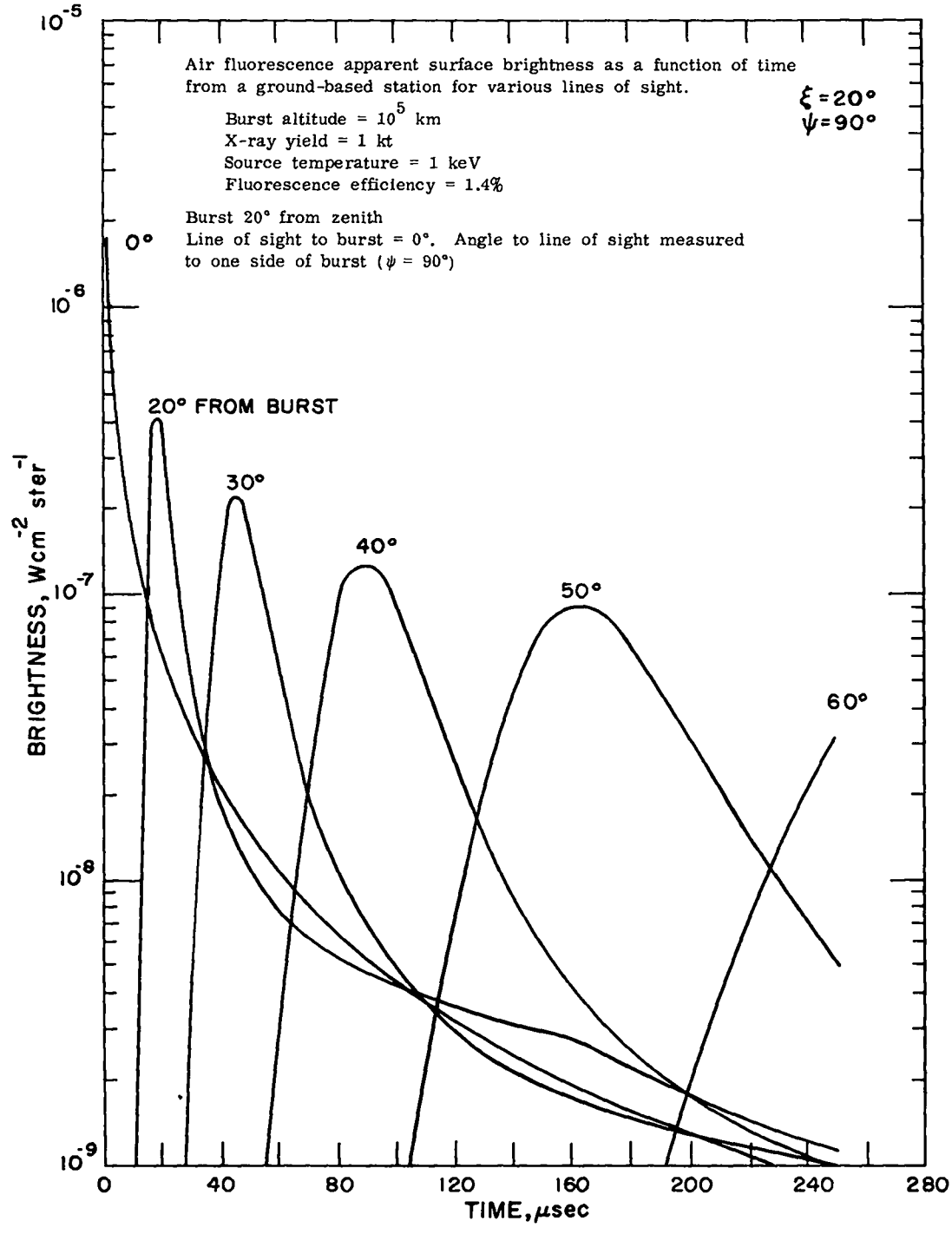

Graph 18 Lines of sight at angles of 0°, 20°, 30°, 40°, 50°, and 60° measured to one side of burst ($\psi = 90°$)

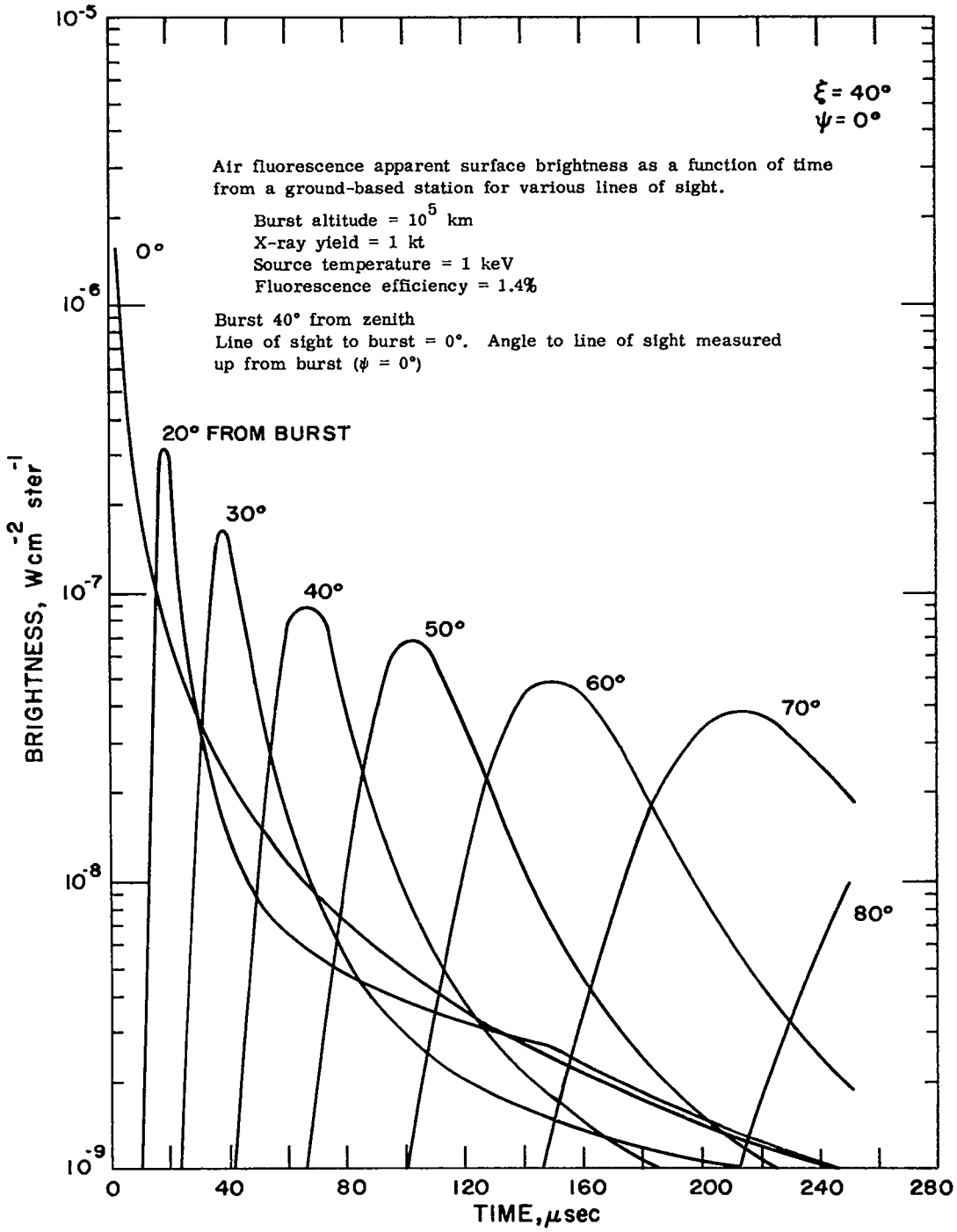

Graph 19 Lines of sight at angles of 0°, 20°, 30°, 40°, 50°, 60°, 70°, and 80° measured up from burst ($\psi = 0°$)

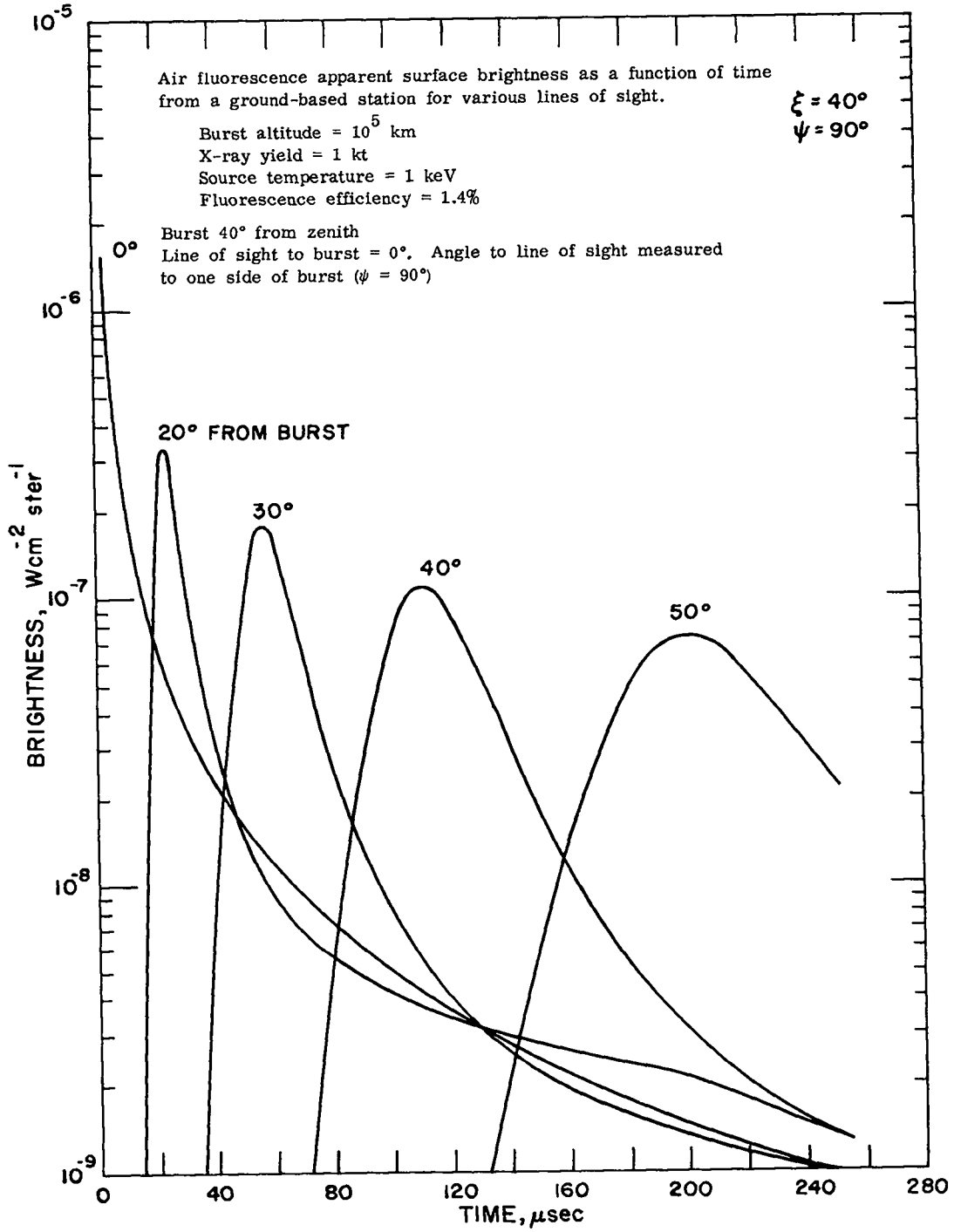

Graph 20 Lines of sight at angles of 0°, 20°, 30°, 40°, and 50° measured to one side of burst ($\psi = 90°$)

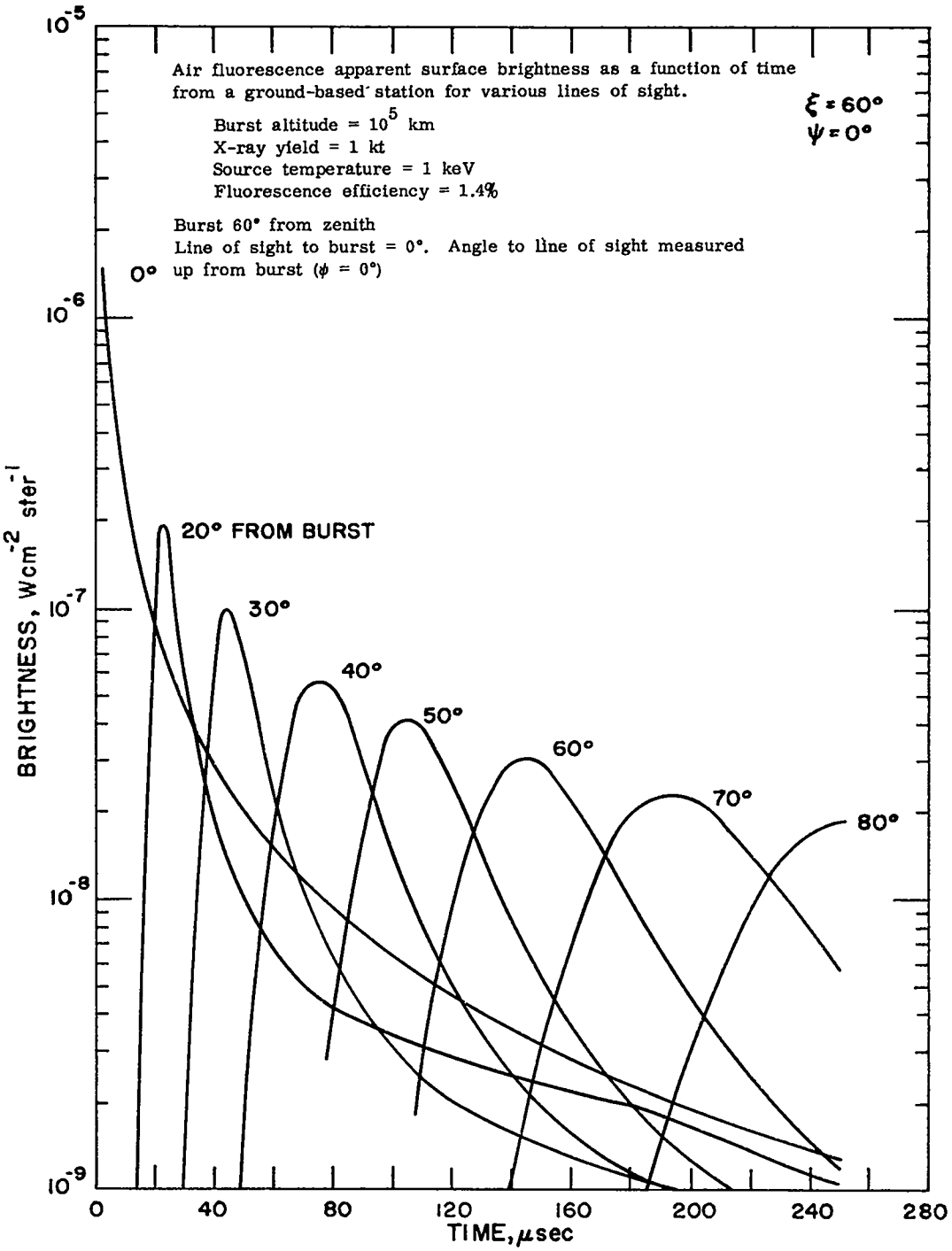

Graph 21 Lines of sight at angles of 0°, 20°, 30°, 40°, 50°, 60°, 70°, and 80° measured up from burst ($\psi = 0°$)

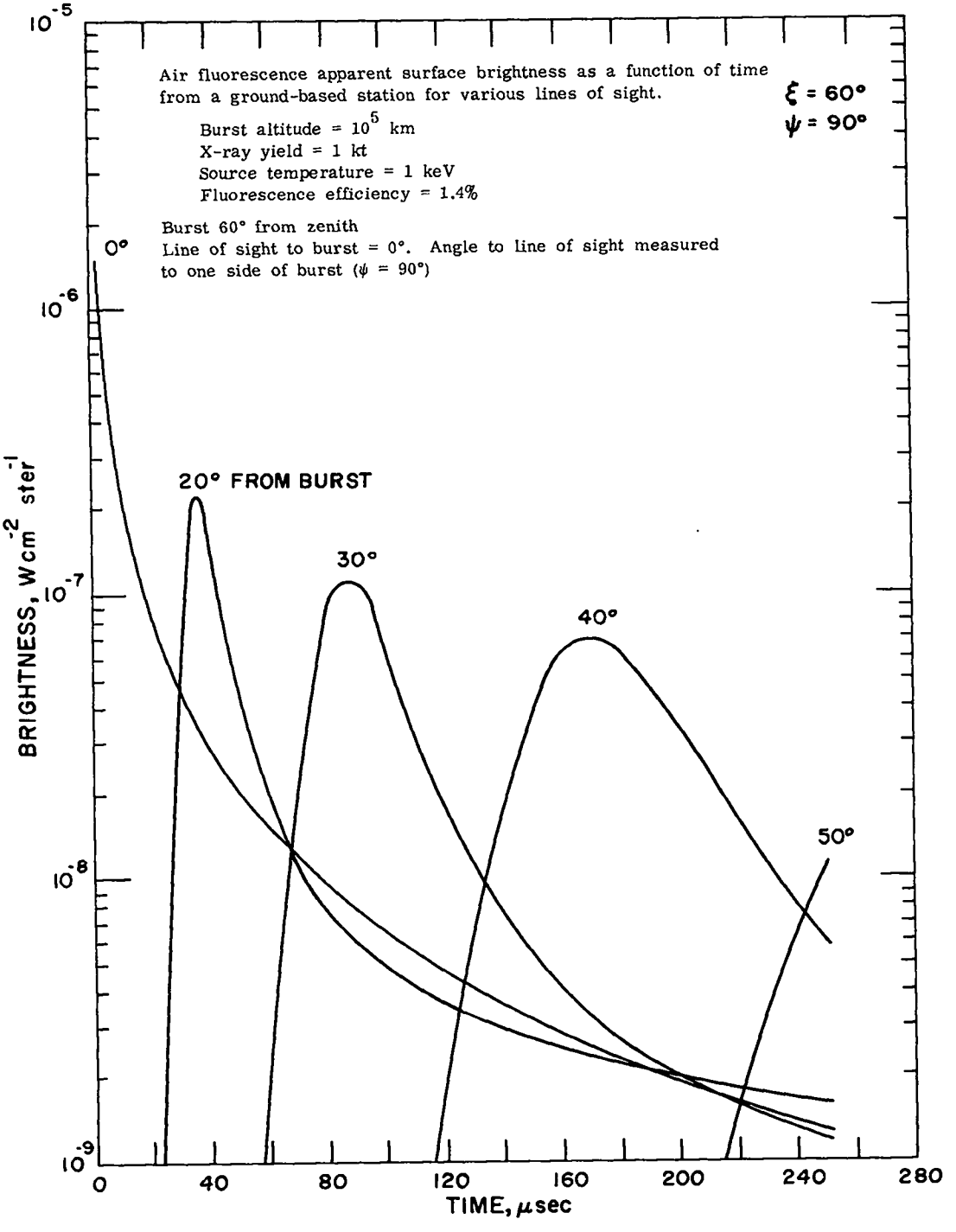

Graph 22 Lines of sight at angles of 0°, 20°, 30°, 40°, and 50° measured to one side of burst ($\psi = 90°$)

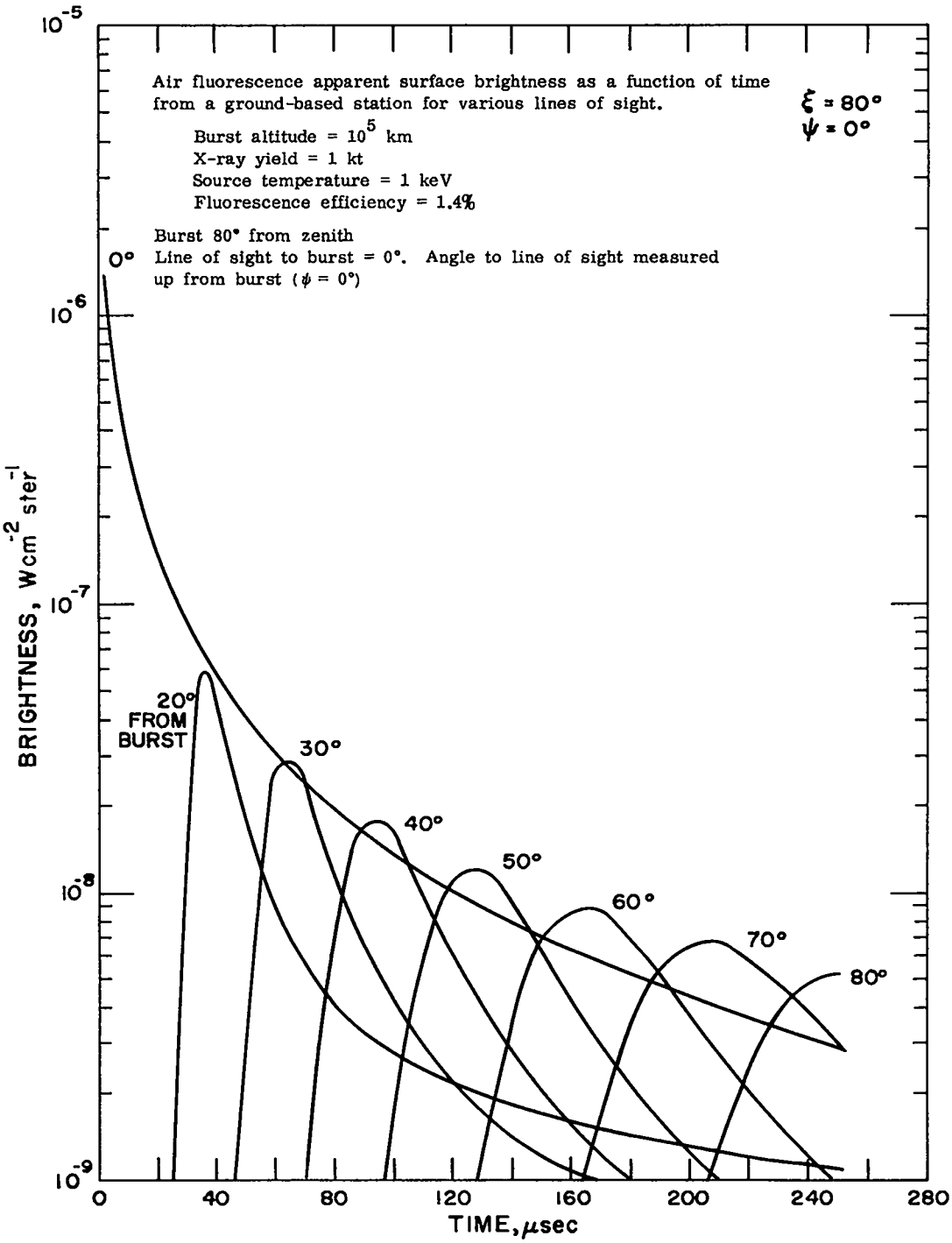

Graph 23 Lines of sight at angles of 0°, 20°, 30°, 40°, 50°, 60°, 70°, and 80° measured up from burst ($\psi = 0°$)

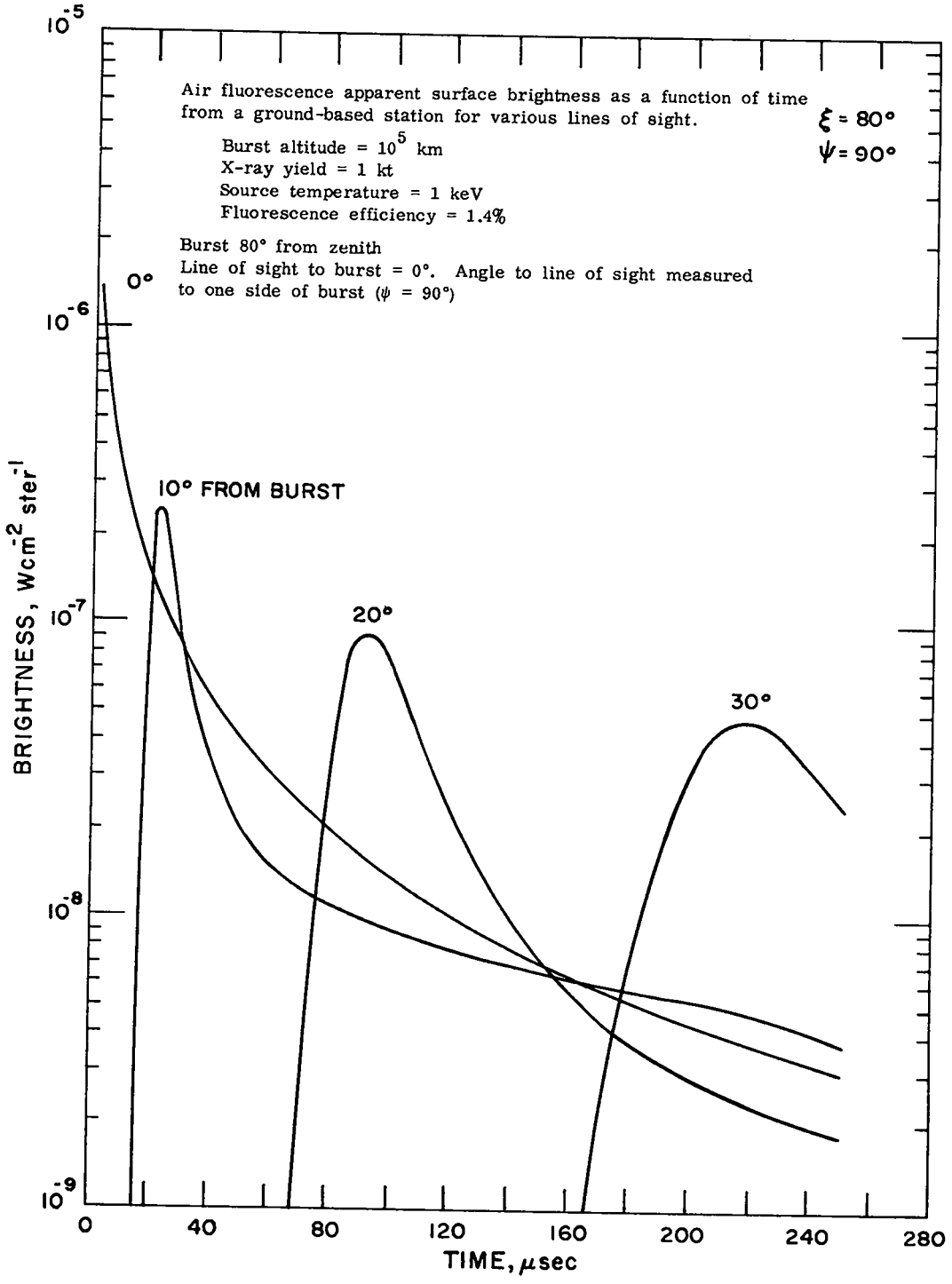

Graph 24 Lines of sight at angles of 0°, 10°, 20°, and 30° measured to one side of burst ($\psi = 90°$)

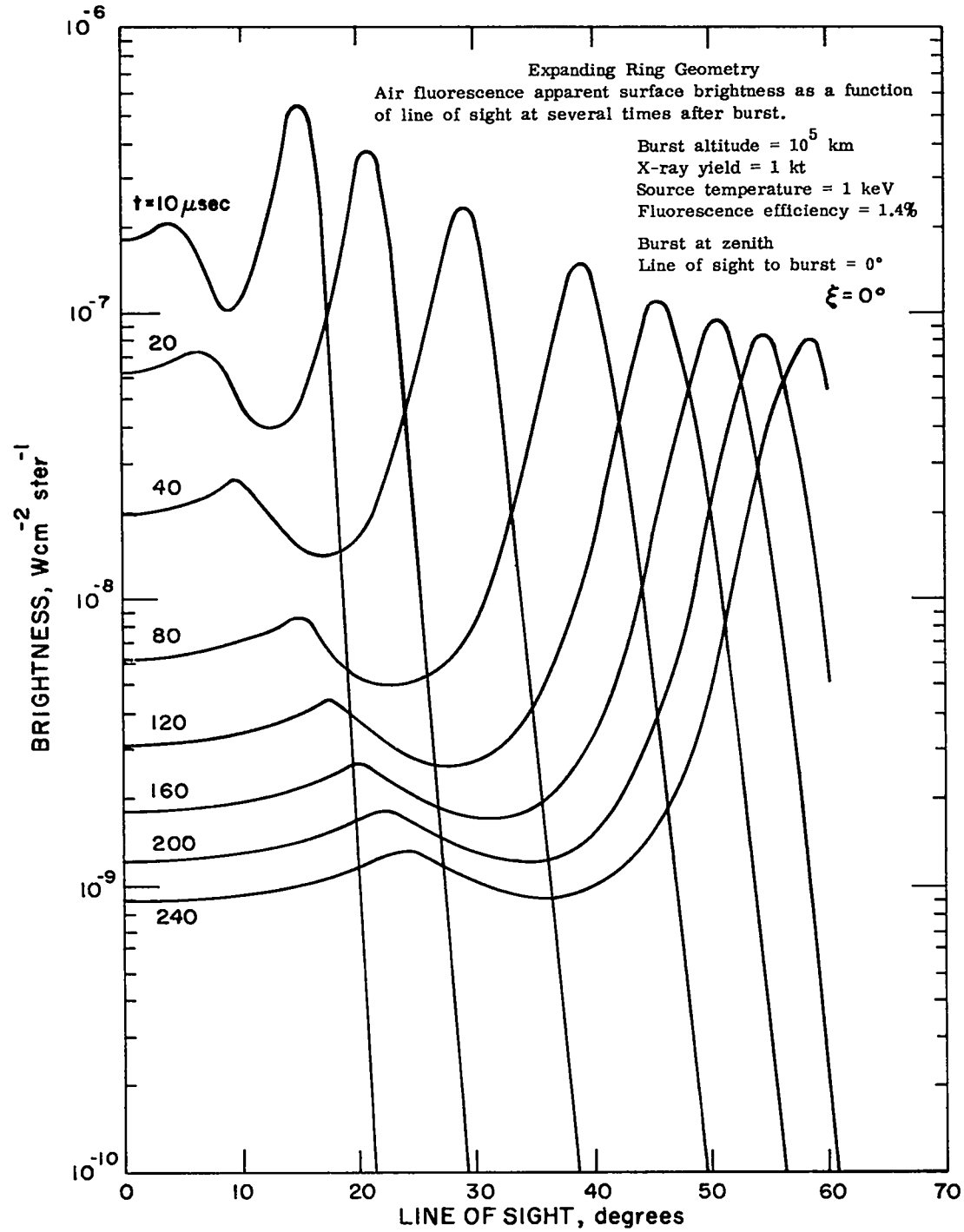

Graph 25 Profiles looking to one side of burst

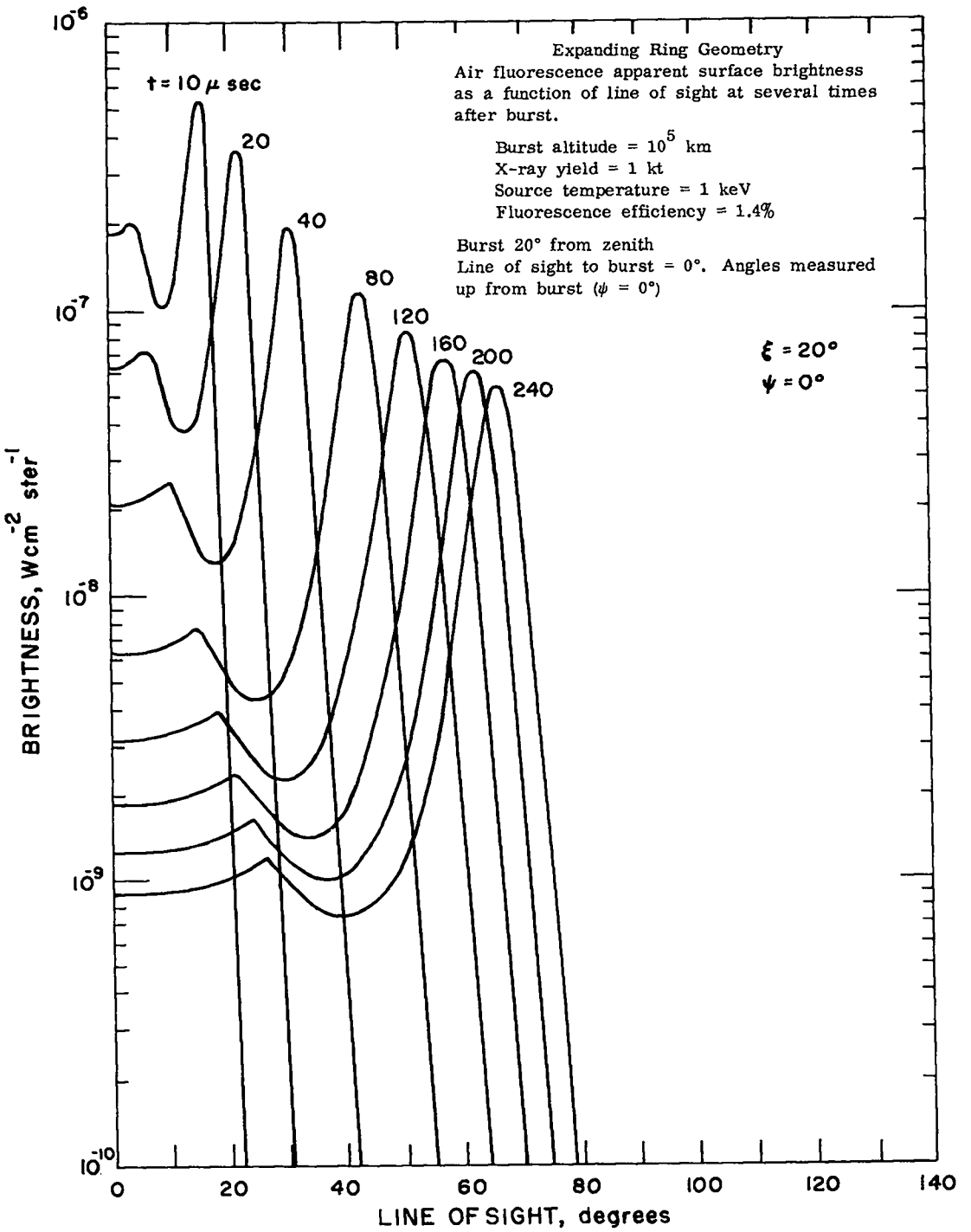

Graph 26 Profiles looking up from burst ($\psi = 0°$)

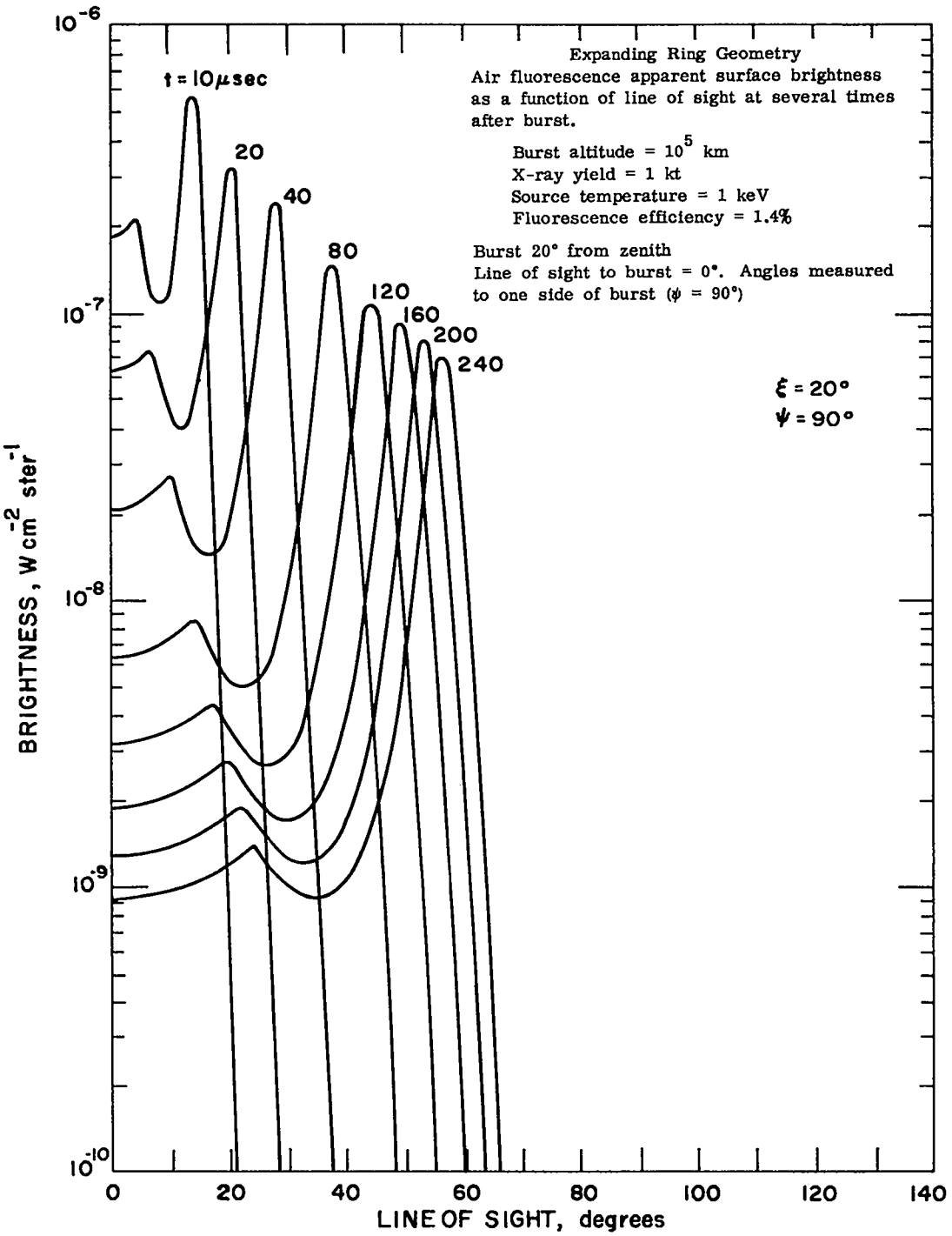

Graph 27 Profiles looking to one side of burst ($\psi = 90°$)

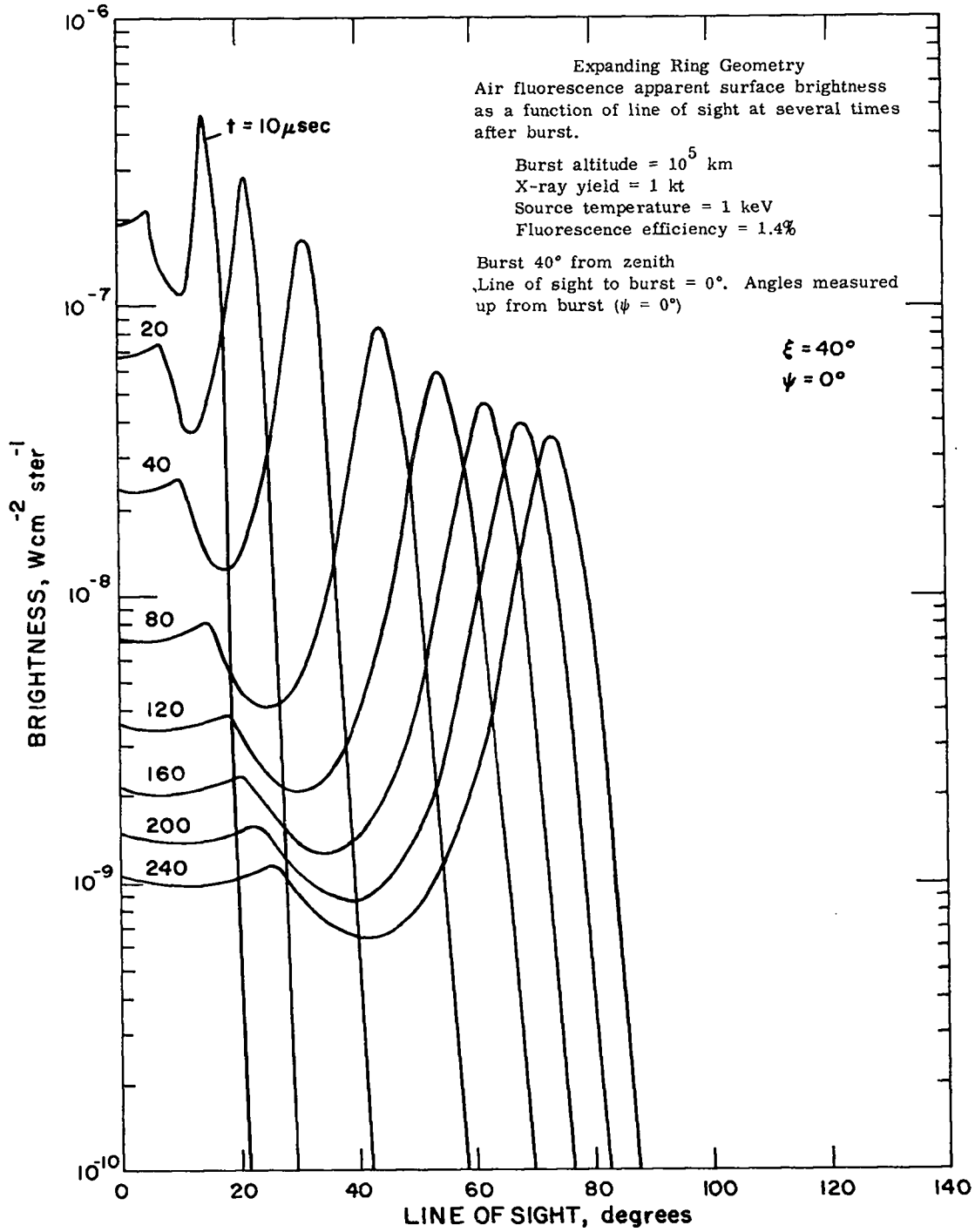

Graph 28 Profiles looking up from burst ($\psi = 0°$)

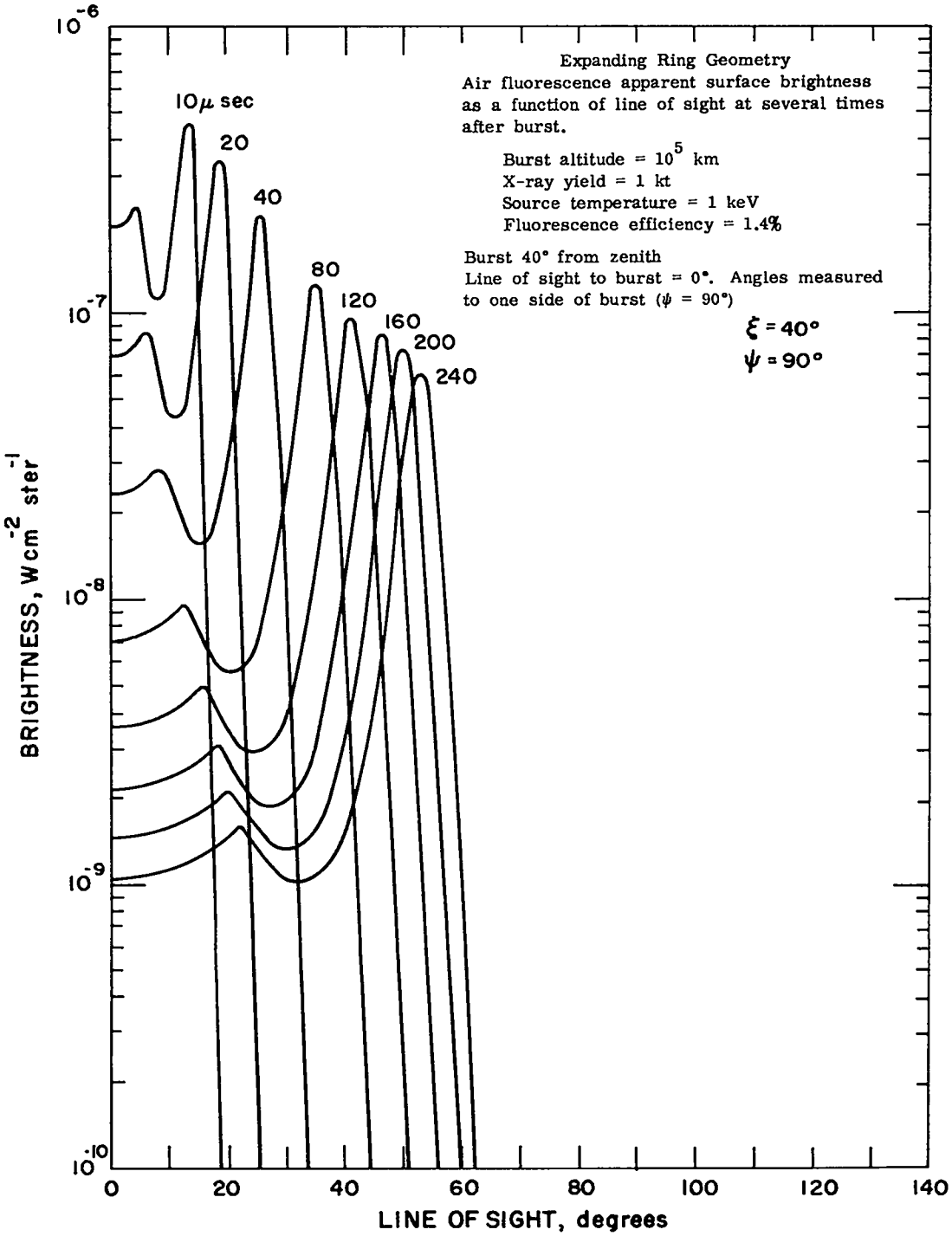

Graph 29 Profiles looking to one side of burst ($\psi = 90°$)

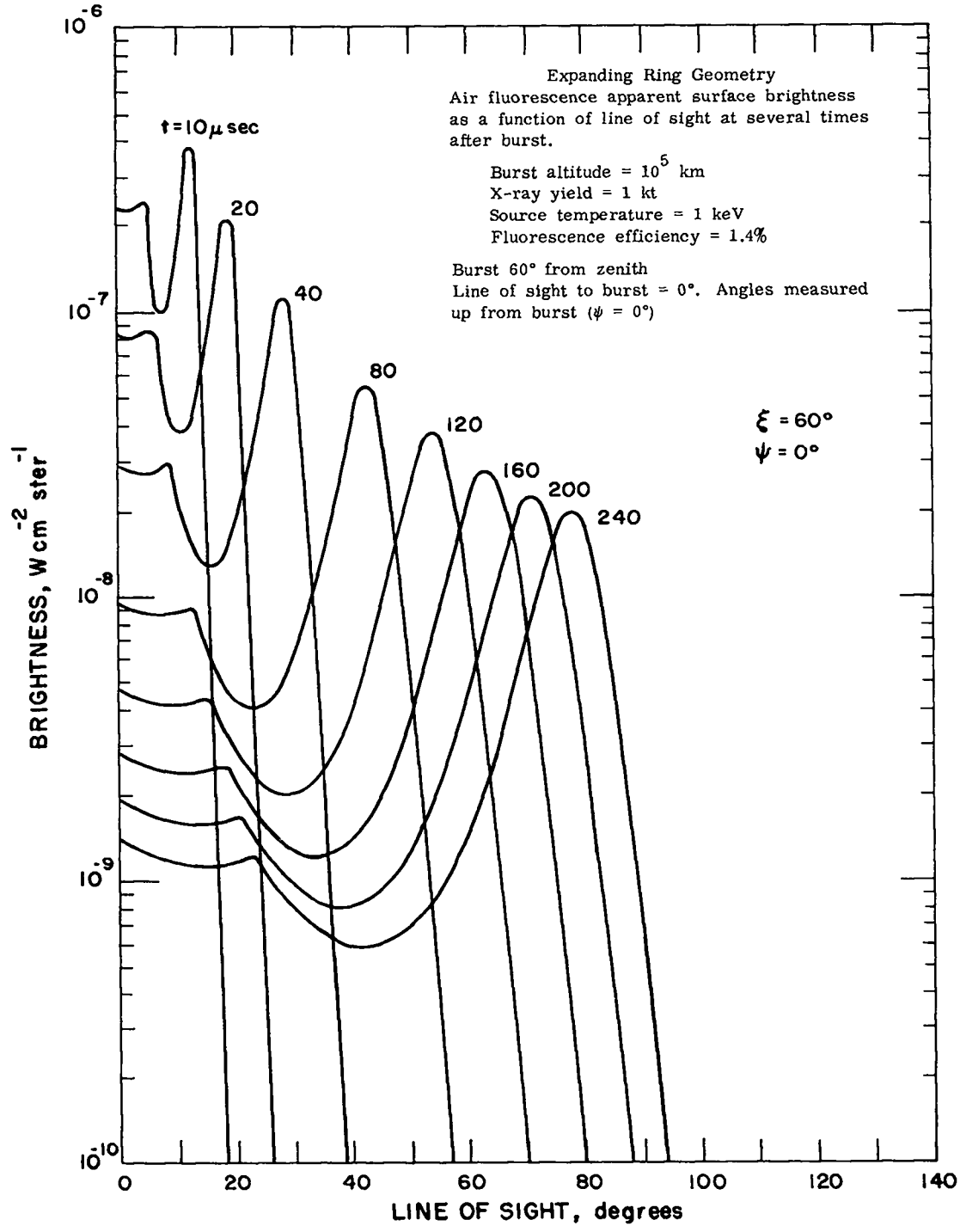

Graph 30 Profiles looking up from burst ($\psi = 0^\circ$)

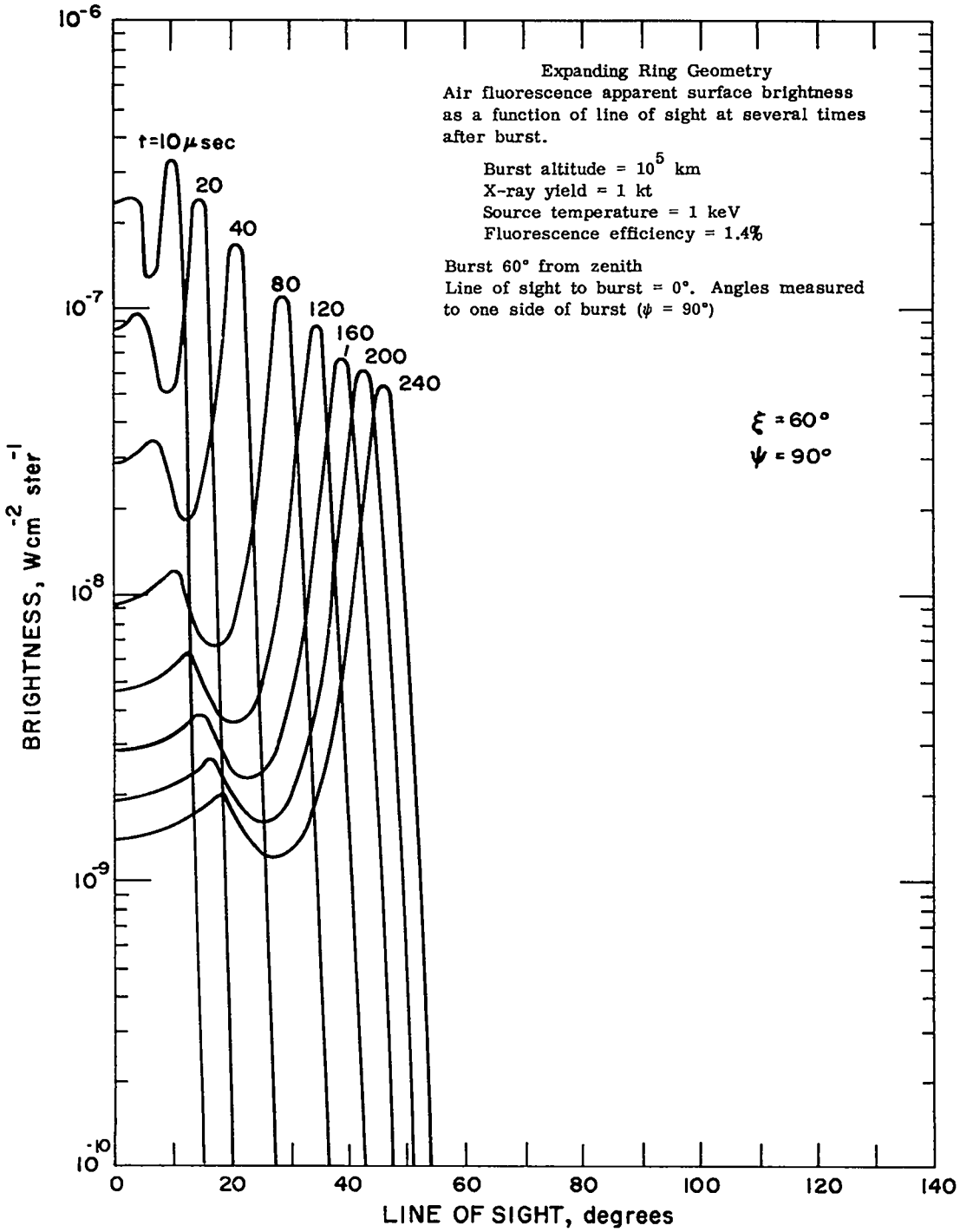

Graph 31 Profiles looking to one side of burst ($\psi = 90°$)

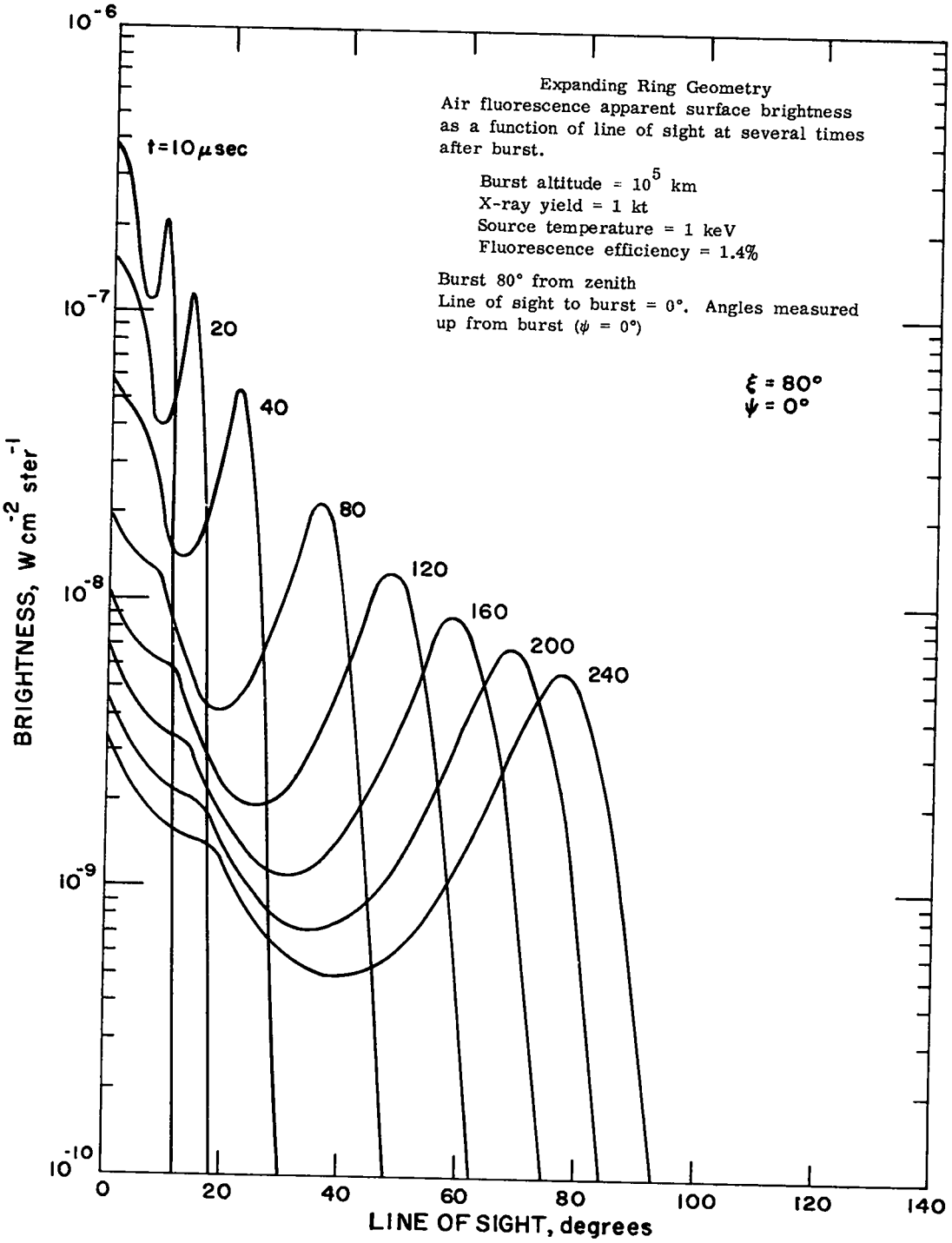

Graph 32 Profiles looking up from burst ($\psi = 0°$)

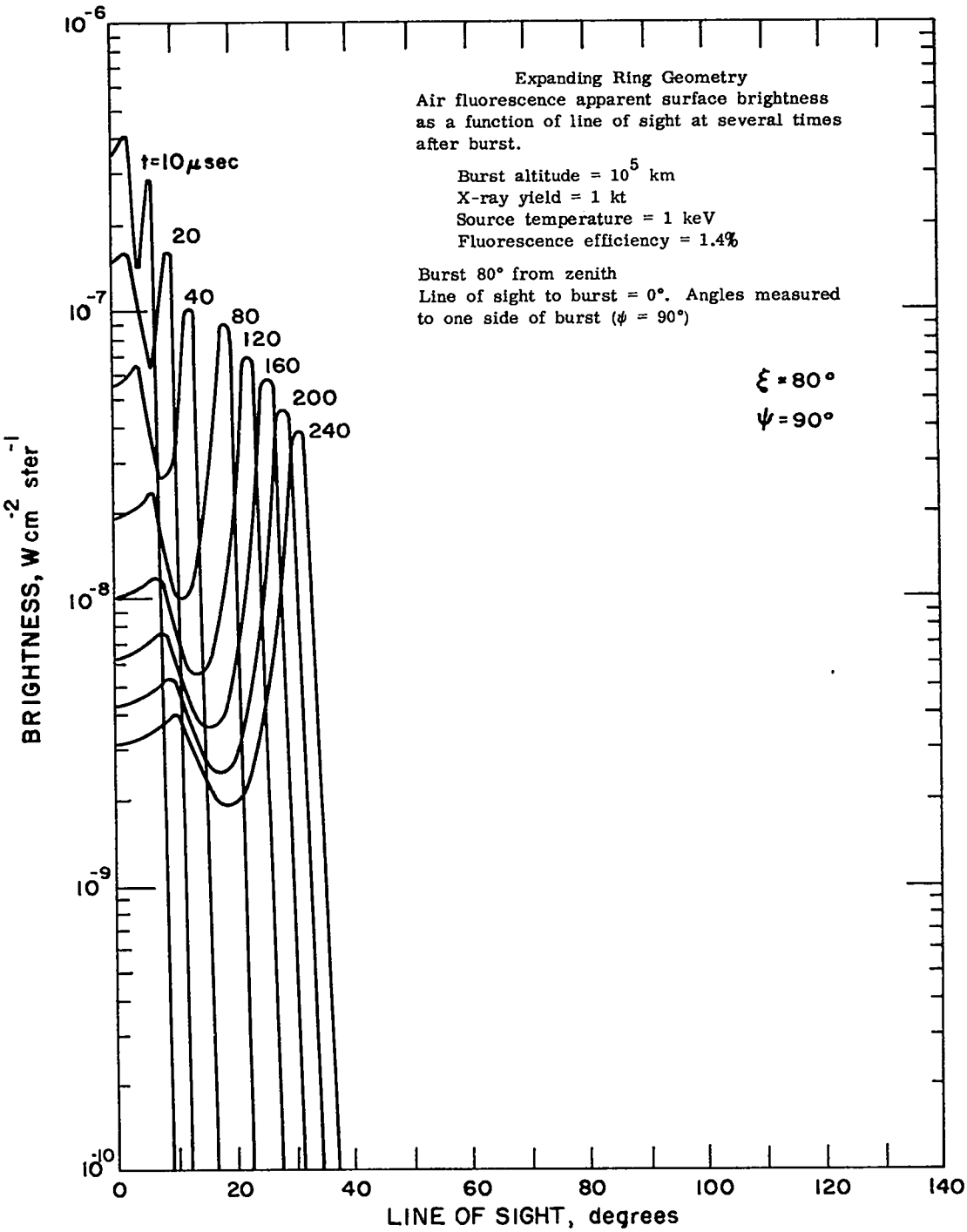

Graph 33 Profiles looking to one side of burst (ψ_r = 90°)

REFERENCES

1. Bennett, E. W., and Holland, R. F., "Prompt Air Fluorescence Excited by High Altitude Nuclear Explosions: Photoelectric Instrumentation and the High Altitude Fluorescence (HAF) and High Altitude Resonance Absorption Calculation (HARAC) Codes," LASL Report LA-3409-MS Supplement, September 1965.

2. Grün, A. E., Can. J. Phys. 36, 858 (1958).

3. Gilmore, F. R., "Graphs of X-Ray Absorption Coefficients for Fourteen Substances," Rand Report RM-2367-AEC, April 1959.

4. Kallman-Bijl, H., et al., Compilers, CIRA 1961, Cospar International Reference Atmosphere, North-Holland Publishing Co., 1961.

5. Bennett, E. W., "Prompt Air Fluorescence Excited by High Altitude Nuclear Explosions: Data and Results (Status Report) Operations Hardtack and Dominic," LASL Report LA-3409-MS, June 1965 (Report Secret, RD).

6. Goldstein, H., and Wilkins, J. E., Jr., "Calculations of the Penetration of Gamma Rays," Atomic Energy Commission Report NYO-3075, Nuclear Development Associates, Inc., 30 June, 1954.

7. Bennett, E. W., "Energy Deposition in the Atmosphere by Delayed Gammas from Fission," LASL Report LAMS-3059, March 1964.

8. Marcum, J. I., "Energy Deposition in the Atmosphere from High Altitude Gamma Ray Sources," Rand Memorandum RM-3594, November 1963.

9. Mjolsness, R. C., and Cashwell, E. D., LASL, private communication.